JGR Biogeosciences

RESEARCH ARTICLE
10.1029/2020JG006209

Special Section:
Ophiolites and Oceanic Lithosphere, with a focus on the Samail ophiolite in Oman

Biogeochemical Gradients in a Serpentinization-Influenced Aquifer: Implications for Gas Exchange Between the Subsurface and Atmosphere

Mary C. Sabuda[1,2,3], Lindsay I. Putman[1,4], Tori M. Hoehler[5], Michael D. Kubo[5,6], William J. Brazelton[7], Dawn Cardace[8], and Matthew O. Schrenk[1,4]

[1]Department of Earth and Environmental Sciences, Michigan State University, East Lansing, MI, USA, [2]Now at Department of Earth and Environmental Sciences, University of Minnesota - Twin Cities, Minneapolis, MN, USA, [3]Now at BioTechnology Institute, University of Minnesota - Twin Cities, Minneapolis, MN, USA, [4]Department of Microbiology and Molecular Genetics, Michigan State University, East Lansing, MI, USA, [5]Exobiology Branch, NASA Ames Research Center, Mountain View, CA, USA, [6]SETI Institute, Mountain View, CA, USA, [7]School of Biological Sciences, University of Utah, Salt Lake City, UT, USA, [8]Department of Geosciences, University of Rhode Island, Kingston, RI, USA

Abstract Serpentinization involves the hydration and alteration of ultramafic rocks, which produces hydrogen (H_2) and methane (CH_4) and results in distinctive groundwater chemistries. As reacted fluids mix with recharging surface water, gradients in chemistry and microbiology develop in the subsurface. We present a comprehensive analysis of biogeochemical gradients in the water column of a serpentinite-hosted well, CSW1.1, at the Coast Range Ophiolite Microbial Observatory (CROMO) in California, USA. Samples for geochemistry, 16S rRNA gene sequencing, and metagenomics were collected at four discrete depths from the top of the well corresponding to 100%, 50%, 15%, and 0% of atmospheric oxygen (O_2) levels, and from the well base at 19.5 m depth. Gibbs energy calculations assessed the energy available for a suite of reactions coupled to O_2, sulfate (SO_4^{2-}), and nitrate (NO_3^-). Metagenomic data from the profile was used to construct metagenome assembled genomes (MAGs) to evaluate the completeness of biochemical pathways and compare the relative abundance of key diagnostic genes. Bioenergetic data point to the favorability of CH_4 oxidation reactions despite little genetic evidence for this. Amplicon sequencing results highlight the abundance of key taxa affiliated with the genera *Truepera*, *Serpentinomonas*, and *Dethiobacter*. Although concentrations of NO_3^- and H_2 are low, genes for NO_3^- reduction and oxidation of H_2 and carbon monoxide (CO) were found in high abundance. Conceptual modeling results demonstrate the net depletion of H_2 and CO in the groundwater, the consumption of CO_2 and O_2, and the potential for CH_4 emission into the atmosphere at this terrestrial site of serpentinization.

Plain Language Summary Microorganisms living in extreme habitats on Earth generate energy by catalyzing chemical reactions using the compounds available. A water-rock interaction known as serpentinization creates high pH and low-oxygen waters, and a limited number of compounds for energy generation. Hydrogen, carbon monoxide, and methane are gases produced through serpentinization that may be used by microorganisms. To unravel small-scale subsurface processes, we studied a depth profile from a serpentinization-influenced groundwater well, and sampled the water at five depths. We measured chemical components of the groundwater (anions, dissolved gases), and calculated the energy available to organisms using a set of common metabolic reactions. We also assessed the microbial communities present, and determined their potential contributions to biogeochemical cycles. We found that three taxa, *Serpentinomonas*, *Truepera*, and *Dethiobacter* dominated. Despite high methane concentrations, genes for methane oxidation were absent throughout the profile. Rather, genes associated with the use of low abundance compounds, like carbon monoxide, hydrogen, and nitrate, were prevalent. This implies that carbon monoxide and hydrogen consumption can deplete these compounds before they reach the surface, and the lack of methane consumption may enable its release into the atmosphere. This work provides insight into the biogeochemical processes mediated by subsurface microorganisms in serpentinization-influenced groundwater.

Key Points:

- Chemical and bioenergetic gradients in ultrabasic groundwater change with depth in well CSW1.1
- Bioenergetic reactions yielding the most energy are incongruent with the functional capabilities encoded within metagenomic data
- 16S rRNA gene sequence data and metagenome assembled genomes reveal that CSW1.1 is dominated by *Serpentinomonas*, *Truepera*, and *Dethiobacter*

Supporting Information:

Supporting Information may be found in the online version of this article.

Correspondence to:

M. O. Schrenk,
schrenkm@msu.edu

Citation:

Sabuda, M. C., Putman, L. I., Hoehler, T. M., Kubo, M. D., Brazelton, W. J., Cardace, D., & Schrenk, M. O. (2021). Biogeochemical gradients in a serpentinization-influenced aquifer: Implications for gas exchange between the subsurface and atmosphere. *Journal of Geophysical Research: Biogeosciences*, *126*, e2020JG006209. https://doi.org/10.1029/2020JG006209

Received 18 DEC 2020
Accepted 7 JUL 2021

Author Contributions:

Conceptualization: Mary C. Sabuda, Tori M. Hoehler, Michael D. Kubo, Matthew O. Schrenk
Data curation: Mary C. Sabuda, Lindsay I. Putman, Michael D. Kubo, William J. Brazelton, Matthew O. Schrenk
Formal analysis: Mary C. Sabuda, Lindsay I. Putman, Michael D. Kubo, William J. Brazelton, Matthew O. Schrenk

Funding acquisition: Tori M. Hoehler, Dawn Cardace, Matthew O. Schrenk
Investigation: Mary C. Sabuda, Lindsay I. Putman, Michael D. Kubo, Dawn Cardace, Matthew O. Schrenk
Methodology: Mary C. Sabuda, Lindsay I. Putman, Tori M. Hoehler, Michael D. Kubo, William J. Brazelton
Project Administration: Matthew O. Schrenk
Resources: Tori M. Hoehler, William J. Brazelton, Dawn Cardace, Matthew O. Schrenk
Software: William J. Brazelton
Supervision: Tori M. Hoehler, Matthew O. Schrenk
Validation: Mary C. Sabuda, Tori M. Hoehler, Michael D. Kubo, William J. Brazelton, Matthew O. Schrenk
Visualization: Mary C. Sabuda
Writing – original draft: Mary C. Sabuda
Writing – review & editing: Mary C. Sabuda, Lindsay I. Putman, Tori M. Hoehler, Michael D. Kubo, William J. Brazelton, Dawn Cardace, Matthew O. Schrenk

1. Introduction

At various tectonic settings along plate boundaries, ultramafic rocks can be uplifted and fractured, allowing water to infiltrate extensively. As hydrothermal fluids interact with these rocks, serpentinization, or the hydration and alteration of ultramafic rock (mainly composed of olivine and pyroxene minerals) occurs. In addition to the formation of the serpentine minerals lizardite, antigorite, and chrysotile, the process of serpentinization produces the magnesium-iron hydroxide mineral brucite, and the iron oxide mineral, magnetite (Mayhew et al., 2013). During the serpentinization of olivine and pyroxene minerals, water and carbon dioxide (CO_2) in solution are reduced to produce hydrogen (H_2) and methane (CH_4), respectively (Etiope, Ehlmann, & Schoell, 2013; McCollom & Seewald, 2013). CH_4 is generated when H_2 reacts with CO or CO_2 via Fischer-Tropsch type reactions (Proskurowski et al., 2008; Schrenk et al., 2013; Suda et al., 2014). The geologic setting and the degree to which serpentinization occurs controls the mineral composition of host rocks and influences surrounding water chemistry.

Natural gradients in water chemistry develop as serpentinization reactions proceed and altered aqueous phases mix with surrounding fluids. Measured waters can range from circumneutral to ultrabasic (pH 10 and above) due to consumption of protons and production of hydroxides. In marine settings, hydrothermal vent systems such as the Lost City Hydrothermal Field are powered by water-rock interactions and extensive fluid cycling between cold ocean water and hydrothermal fluids. There, dissolved ions in seawater (e.g., sulfate (SO_4^{2-}), chloride (Cl^-), magnesium, sodium) can interact with the ultrabasic waters associated with serpentinization, creating stark geochemical gradients and unique environments that sustain life (Brazelton et al., 2006; McGonigle et al., 2020; Motamedi et al., 2020; Schrenk et al., 2013). In the lagoon marine environment of the Prony Hydrothermal Field in New Caledonia, high pH and low salinity hydrothermal fluids of terrestrial origin discharge via carbonate chimneys into shallow seawater which creates steep geochemical gradients (Monnin et al., 2014). Depending on the chimney and its structure, microbial community compositions varied (Quéméneur et al., 2014). In the inner parts of the chimneys, *Firmicutes* and *Chloroflexi* dominated CH_4- and H_2-rich anoxic fluids. In oxic-anoxic transition zones, the H_2-oxidizing chemolithoautotrophic *Hydrogenophaga* was identified as an important genus (Quéméneur et al., 2014).

Similarly, in settings where the seafloor has been uplifted onto continents (i.e., ophiolites), meteoric water can percolate into the subsurface and mix with ultrabasic serpentinite aquifers and remnant seawater. Serpentinite-hosted groundwater within ophiolite sequences are becoming well-studied throughout the world in locations such as Oman (Chavagnac et al., 2013; Miller et al., 2016), Italy (Brazelton et al., 2017; Schwarzenbach et al., 2012), Canada (Morrill et al., 2014), the Philippines (Cardace et al., 2015; Meyer-Dombard et al., 2015; Woycheese et al., 2015), Japan (Merino et al., 2020), and Costa Rica (Sanchez-Murillo et al., 2014; Schwarzenbach et al., 2016) for various environmental (Aloupi et al., 2012; Baes & McLaughlin, 1987), astrobiological (McKay et al., 2014; Rempfert et al., 2017; Szponar et al., 2013), and economic (Holloway et al., 2009) purposes.

Work at The Cedars in California, USA has shown oxic to anoxic transitions and stratification with depth in ultrabasic springs due to the presence of both meteoric water input at the surface and serpentinization-influenced groundwater infiltration at the base (Suzuki et al., 2013). This observation was reflected in microbial community composition, where 16S and 18S rRNA gene sequencing revealed that pools fed by the deeper groundwater source had distinct communities and also more uncharacterized candidate phyla relative to the surface waters (Suzuki et al., 2013). Research at the Samail ophiolite in Oman examined the geochemistry and microbiology between wells along the ophiolite sequence (Rempfert et al., 2017). There, wells upgradient of the groundwater flow path sampled an open system with a shallow water source measuring pH 8–9 (alkaline fluids) and downgradient wells sampled a closed system with a deeper water source measuring pH > 10 (hyperalkaline fluids; Rempfert et al., 2017). Both upgradient and downgradient wells sampled partially serpentinized peridotite, but further down the ophiolite sequence, monitoring wells sampled peridotite-gabbro contact fluids and gabbro-only fluids. Upgradient alkaline fluids here were more oxidized, with relatively higher dissolved inorganic carbon (DIC), SO_4^{2-} and NO_3^-, but no detectable CH_4 or H_2. In addition to pH, downgradient hyperalkaline fluids were characterized by high quantities of calcium (Ca^{2+}), H_2, and CH_4 concentrations, but were depleted in magnesium, SO_4^{2-}, NO_3^-, DIC and silica. While these studies assessed their own version of hydrologic gradients, to date, no study has directly assessed depth-resolved in situ biogeochemical gradients in a serpentinizing groundwater well.

While many studies of serpentinizing systems sample surficial springs influenced by atmospheric processes as described above, the monitoring wells located at the Coast Range Ophiolite Microbial Observatory (CROMO) in California sample isolated fluids hosted within a confined serpentinite aquifer (Ortiz et al., 2018). Within the main aquifer, fluids show a greater influence of serpentinization with depth. Shallow wells have circumneutral pH whereas the wells drilled to intermediate and greater depths are more heavily influenced by ultrabasic fluids, contain less oxygen, lower oxidation-reduction potential (ORP), higher conductivity, and increased SO_4^{2-}, Cl^-, and CH_4 (Sabuda et al., 2020). Most wells sample deeper, more isolated waters and provide a window into this extreme ecosystem. Compared to other serpentinizing systems such as the Samail ophiolite (i.e., Miller et al. (2016); 0.18 mM at NSHQ04-18m), dissolved H_2 at CROMO is chronically depleted (Twing et al., 2017; 0.29 μM in CSW1.1).

Microbial community composition varies at CROMO and appears to be driven by changes in pH, dissolved oxygen, nutrient composition, and dissolved gases (Crespo-Medina et al., 2014; Twing et al., 2017). Microcosm experiments inoculated with CROMO fluids, a H_2 atmosphere, and a carbon source (CO_2, CH_4, acetate (CH_3COO^-), or formate) revealed bacterial growth when inoculated with CH_4 and acetate (Crespo-Medina et al., 2014). Results also showed that the addition of nutrients or electron acceptors had no significant effect on the growth of organisms, except for the addition of polysulfides, where community compositions changed to favor *Dethiobacter* and members of the Comamonadaceae family (Crespo-Medina et al., 2014). Similarly, work by Twing et al. (2017) showed pH, CO, and CH_4 best explained the variability in bacterial community composition across the site, with positive correlations between both *Dethiobacter* and members of the Comamonadaceae family to CH_4 ($p \leq 0.05$). Metagenomic data and metagenome assembled genomes (MAGs) from the CROMO fluids provided evidence for carbon fixation pathways such as CH_4 oxidation to formaldehyde, the Calvin-Benson-Bassham cycle (CBB), and the reductive acetyl coenzyme A (acetyl-CoA; Wood-Ljungdahl) pathway (Seyler et al., 2020).

Similar carbon transformation capabilities have been identified at other sites of continental serpentinization. For example, at the hyperalkaline springs within the Santa Elena ophiolite in Costa Rica, metagenomic evidence for methane production and consumption was identified and were suggested to have impacts on the resulting gas flux out of the system (Crespo-Medina et al., 2017). At a site of serpentinization in the Tablelands ophiolite in Newfoundland, Canada, laboratory experiments were conducted with ultrabasic fluids, sediment, and carbon amendments (Morrill et al., 2014). These experiments showed that methanogenesis did not happen in experiments where bicarbonate, formate, acetate, or propionate were added. Rather, stable isotope probing of $\delta^{13}C$ showed CO utilization, potentially by organisms related to *Hydrogenophaga,* especially in mixing zones where serpentinizing groundwater interacts with the atmosphere (Morrill et al., 2014).

In this study, we use field geochemical measurements, Gibbs energy calculations, 16S rRNA gene sequence data, metagenomic data, and high quality MAGs to investigate the distribution and metabolic potential of microorganisms in the context of biogeochemical gradients with depth in the CSW1.1 well at CROMO. We gain insight into how variations in chemistry impact the distribution and function of microbial communities within this extreme environment. Microbial populations in these environments must obtain energy for survival and growth in the high pH, low-oxygen fluids, and as such, it is critical to understand how these communities interact and capitalize upon chemical variances. We further consider the physiological capabilities of microbial communities of microbial populations in the serpentinizing subsurface, as represented in their (meta-) genome composition. Finally, with the combined geochemical, energetic, and metagenomic data, we reflect on the possibility for gas exchange between the subsurface and atmosphere in this groundwater well, while recognizing future work is needed to specifically quantify gas fluxes. This is the first study that has combined aqueous geochemical measurements, microbiological characterization, and thermodynamic calculations to develop a comprehensive profile as a function of depth in a serpentinite-hosted groundwater well.

2. Materials and Methods

2.1. CSW1.1 Water Column Sampling

The water column of the CSW1.1 well was characterized in May 2016 for its aqueous geochemistry and microbiology at four distinct locations according to O_2 concentrations. To best identify gradients that had formed in the top of the well since the previous sampling point in January 2016, the well was not pumped to exchange for fresh fluids before sampling. For more details about the location of CSW1.1 and the CRO-MO field site, see Ortiz et al. (2018). Dissolved O_2 equal to 100%, 50%, 15% and 0% air saturation were determined using an ultrasensitive Orion Dissolved Oxygen Probe (ThermoScientific), and sterile Tygon tubing (Sigma-Aldrich), which allowed samples to be extracted from these discrete depths once reached. An ethanol-rinsed (70%) water level meter (Solinst) was simultaneously deployed to monitor the depth of each discrete air saturation level, and all three devices were zip tied together and sterilized with 70% ethanol before lowering into the well. A schematic of this sampling setup is shown in Figure S1. The interior PVC casing radius of the CSW1.1 well (0.0508 m), was used to calculate the theoretical maximum water volume extractable for each depth profile sample to avoid disturbance to the remaining deeper column samples (i.e., when sampling 100% O_2 level, avoid disturbing the deeper 50%, 15% or 0% O_2 levels). As each dissolved oxygen (DO) concentration was reached, 60 mL of water was collected to obtain estimates for pH, oxidation-reduction potential, specific conductance, and temperature using a separate digital YSI probe. DO detection limits were 0.002 mg/L for the ultrasensitive probe and 0.157 mg/L for the YSI meter, as calculated using May 2016 data. Well fluids at each interval were pumped through the tubing until it came out the other side, then fresh fluids were collected for quantification of anions (Br^-, Cl^-, NO_2^-, NO_3^-, and SO_4^{2-}), total HS^-, DIC, and dissolved gases. Additionally, samples were collected at each depth for metagenomic analysis and determination of cell and 16S rRNA gene sequence abundances, using the methods detailed below.

Water was also pumped from the base of the CSW1.1 well (19.5 m) in May 2016 after exchanging for fresh fluids as previously described (Crespo-Medina et al., 2014; Sabuda et al., 2020; Twing et al., 2017), with a few modifications as briefly explained here. Fluids were sampled from the bottom of the well via a pre-installed Teflon bladder pump (Geotech Environmental Equipment) and sterile tubing, and samples were directly collected for fluid chemistry. A digital YSI multiprobe was used to collect pH, ORP, DO, specific conductance, and temperature measurements after dissolved O_2 readings stabilized.

2.2. Geochemistry

Fluids for anion analysis were preserved by passage through 0.2 μm Sterivex syringe filters (Millipore, Billerica, MA, USA), collected in 25 mL HDPE bottles, and stored at 4°C until analysis via ion chromatography. Triplicate samples were measured on a Dionex ICS-2100 Ion Chromatography System (ThermoScientific). Total HS^- was determined via UV spectrophotometry using the methylene blue method (Cline, 1969; Text S1).

Dissolved gases (H_2, CH_4, CO) were extracted in the field by vigorously shaking a known volume of anoxic sample fluid with a known volume of N_2 gas in a 60 mL syringe attached to a stopcock. The headspace gas was transferred via a needle to a 15 mL glass vial that was completely filled with a 200 ppt sodium chloride solution and capped with a 20 mm thick butyl rubber stopper to store the gas until analysis. Sample vials were stored upside down to avoid any potential gas exchange with the stopper. Gas samples were analyzed within hours for concentrations of H_2 and CO via a Trace Analytical RGA3 Reduced Gas Analyzer, and within days for concentrations of CH_4 with a SRI 8610C gas chromatograph-flame ionization detector (GC-FID). The detection limit for all of these gases was 0.003 μM (Crespo-Medina et al., 2014).

Fluids for DIC analyses were collected by filtration through 0.2 μm syringe filters into nitrogen (N_2) flushed 125 mL glass serum bottles (Wheaton Industries, Inc.) fitted with a 20 mm thick blue butyl stoppers (Chemglass Life Sciences) with a vent needle inserted to allow excess N_2 headspace to escape. Samples were acidified within the sealed vials in the field using 3 mL concentrated phosphoric acid. Quantification of DIC was performed by measuring the concentration of liberated CO_2 in the headspace using GC-FID (SRI 8610C). The GC employed an inline "methanizer" device that converts CO_2 to methane and thereby significantly increases the sensitivity of detection via flame ionization detector (Twing et al., 2017).

2.3. Gibbs Energy Calculations

We calculated the Gibbs energy change associated with reactions involving H_2, CH_4, CO, and acetate as electron donors and O_2, NO_3^-, and SO_4^{2-} as electron acceptors using measured fluid chemistries (Table S1). Total HS^- was only detected in samples from the bottom of the well. At all other sampled depths HS^-, NO_2^- and NO_3^-, were calculated using the detection limit of 1 μM. Acetate was not analyzed for these samples due to limitations on extractable water volume at each depth, and was conservatively estimated at 1 μM, which lies well below previously measured concentrations from Crespo-Medina et al. (2014) (57.8 μM) and Twing et al. (2017) (70.79 μM). Where detection limits were used, the respective calculations serve as a lower limit on energy availability within CSW1.1. In order to assess dissimilatory nitrate reduction to ammonia (DNRA), ammonium concentrations from Crespo-Medina et al. (2014) were used to estimate available ammonium within the well. As previously measured formate concentrations in Twing et al. (2017) are roughly 1/6 the concentration of acetate, they were not considered in the current calculations.

$$\Delta G = \Delta G^0 + RT\ln Q \quad (1)$$

Gibbs energy change was calculated according to Equation 1 above, where ΔG^0 is the Standard Gibbs Energy change of reaction (J/mol), ΔG is the Gibbs Energy change under *in situ* conditions (J/mol), R is the universal gas constant, 8.3145 (J/mol · K), T is the temperature (Kelvin), and Q is the reaction quotient of the compounds involved in the respective reaction. The reaction quotient was calculated using the activities established by fluid speciation calculations performed using Geochemist's Workbench© (Aqueous Solutions LLC) that accounted for high pH conditions. ΔG^0 values for the selected reactions were cited from the work of Amend & Shock, 2001, or manually calculated using their ΔG values for components of the reaction when the ΔG^0 was not available from their work. ΔG (kJ/mol) values were normalized to the number of electrons transferred in any given reaction by dividing ΔG values by the number of electrons transferred within a reaction. Volumetric available energy (ΔG mJ/L) was also calculated by accounting for the concentration of the limiting reactant within a reaction (McCollom & Shock, 1997).

2.4. Cell Abundance

Unfiltered water for cell counts was collected in sterile 15 mL Falcon tubes (Fisher Scientific) and fixed with 3.7% formaldehyde. Triplicate samples were preserved and stored at 4°C until analysis. Cells were collected on 0.2 μm black polycarbonate filters (Millipore) and a 1 μg/mL 4′,6-diamidino-2-phenylindole solution was applied. An epifluorescence microscope (Olympus) was used to count cells according to previously published protocols (Schrenk et al., 2003).

2.5. 16S rRNA Gene Amplicon Sequencing and Data Analysis

At each profile sampling interval, water samples (400 mL) were collected immediately for 16S rRNA gene sequencing using 0.2 μm Sterivex filters (Millipore) on ice attached directly to the sterile Tygon tubing. At the well bottom, 4L of water was filtered through 0.2 μm Sterivex filters as performed historically during CROMO sampling (Twing et al., 2017). The filters were immediately capped and frozen in liquid nitrogen before storage at −80°C. DNA was extracted from Sterivex filters using phenol/chloroform extractions and precipitated with ethanol as previously described (Sabuda et al., 2020; Twing et al., 2017). Following extraction, DNA extracts were purified using the Genomic Clean and Concentrate Kit (Zymo Research), and quantified using a Qubit dsDNA High Sensitivity Assay kit on a Qubit 2.0 fluorometer (ThermoFisher). Blanks and extraction blanks were collected, but did not amplify via PCR and were not submitted for sequencing. More details about amplification of bacteria and archaea are presented in the supporting information (Text S2).

Purified genomic DNA samples were submitted to the Genomics Core Facility at Michigan State University for analysis and processed on an Illumina MiSeq instrument to amplify the V4 region of the 16S rRNA gene (515F: GTGCCAGCMGCCGCGGTAA/806R:GGACTACHVGGGTWTCTAAT primers) using dual indexed Illumina fusion primers (Kozich et al., 2013). Products were normalized and pooled using an Invitrogen SequalPrep DNA Normalization Plate and then loaded on an Illumina MiSeq v2 flow cell and sequenced

using a standard 500 cycle reagent kit after library quality control and quantitation was performed. Illumina Real Time Analysis (RTA) software v1.18.54 performed base calling, and using Illumina Bcl2fastq (v1.8.4), the RTA output was demultiplexed and converted to FastQ files.

Paired-end sequence reads were filtered and merged using USEARCH 8 (Edgar, 2010) with additional quality filtering in Mothur (Schloss et al., 2009) to remove sequences with ambiguous bases and more than 8 homopolymers. Chimaeras were removed with Mothur's implementation of UCHIME (Edgar et al., 2011) before sequences were pre-clustered with the Mothur command pre.cluster (diffs = 1), which removes rare sequences most likely created by sequencing errors (Schloss & Westcott, 2011). The final unique sequence types were considered to be the operational taxonomic units (OTUs) (Brazelton et al., 2017). The SILVA SSURef alignment (v132) was used to align sequences, and taxonomy was assigned using Mothur (Pruesse et al., 2007; Schloss et al., 2009), as described in Twing et al. (2017).

Filtering of common contaminants was applied to the 16S rRNA gene fasta file ((266,833 OTUs); 1,426,293 reads) based on common contaminant taxa identified in Census of Deep Life samples by Sheik et al. (2018) and previous work by Fullerton et al. (2021). First, singletons (81,326 OTUs; 22,236 reads) were removed to focus on more abundant taxa involved in biogeochemical cycling trends. Sequences identified as eukaryotes (2,277 OTUs; 3,805 reads), archaea (1,477 OTUs; 4,573 reads), mitochondria (254 OTUs; 1,391 reads), chloroplasts (2,089 OTUs; 9,414 reads), and unknown (2,600 OTUs; 6,061 reads) by SILVA were removed. A total of 18,178 OTUs; 76,819 reads were identified as potential common contaminants of deep subsurface samples and thus removed. Manual curation and analysis of the abundance and distribution of potential contaminants removed an additional 5,415 OTUs and 28,498 reads were identified as contaminant OTUs were removed from the data set. OTUs removed from the data set are listed in Data Set S3. The resulting 16S rRNA gene data set contains 159,647 OTUs and 1,275,154 reads (89.4% of original reads). Richness and Pielou's evenness alpha diversity metrics were calculated using the Shannon Index in *R* (R Core Team, 2019) using the vegan package v.2.5–6 (Oksanen et al., 2019).

2.6. Metagenome Analysis

For the CSW1.1 depth profile, metagenome sequencing was performed at the University of Utah. Metagenome libraries were constructed with 80 ng of purified DNA that was fragmented by sonication with a Q800R sonicator (Qsonica) at 4°C, 25% amplitude, with a 10-second pulse for 60 s. Magnetic beads (Rohland & Reich, 2012) were used to select fragmented DNA with a size range of 500–700 bp. Libraries were prepared with the NEBnext Ultra DNA library prep kit for Illumina according to manufacturer instructions. Quality control and sequencing of the metagenomic libraries was conducted at the University of Utah High-Throughput Genomics Core Facility. Libraries were evaluated for quality on a Bioanalyzer DNA 1000 chip (Agilent Technologies), and then paired-end sequencing (2 × 125 bp) was performed on an Illumina HiSeq2500 platform with HiSeq v4 chemistry. The seven CSW1.1 depth profile libraries were multiplexed and pooled into one lane of Illumina sequencing. Demultiplexing and conversion of the raw sequencing base-call data were performed through the CASAVA v1.8 pipeline. Quality control of the sequencing reads was performed as described in Thornton et al. (2020), and the final set of quality-controlled sequences represented 70%–77% of all original reads in each library. Co-assembly of the CSW1.1 depth profile quality-controlled sequences was performed with Megahit v1.1.1 (Li et al., 2016) with parameters kstart = 27, kend = 127, and kstep = 20.

All contigs were included for protein prediction and annotation, with a minimum length of 200 bp. Putative coding DNA sequences were predicted with Prodigal v2.6.3 (Hyatt et al., 2010) in meta mode. Predicted protein sequences were annotated by searching against KEGG release 83.2 (Ogata et al., 1999) using Diamond v0.9.14 (Buchfink et al., 2014). Coverage of predicted proteins was calculated as described by Thornton et al. (2020) and briefly described here. Quality-controlled sequence reads were mapped to the co-assembly with Bowtie2 v2.3.2 (Langmead & Salzberg, 2012) with the very-sensitive flag, and the results were sorted by name using Samtools v1.3 (Li et al., 2009). All samples had bowtie2 overall alignment rates of 98%–99% to the pooled assembly. The coverage for each predicted protein-coding gene was calculated as fragments per kilobase of target per million mapped reads (FPKM) with count_features v1.3.0, part of the seq-annot package (Thornton et al., 2020). FPKM values are normalized to the length of the predicted protein sequence and are ideal for comparisons within samples. Comparisons of FPKM between samples can be problematic,

but the patterns in Table 2 should be fairly robust to choice of coverage units due to the high mapping rate to the pooled assembly.

MAGs were binned with BinSanity (Graham et al., 2017) using the low-memory Binsanity-lc (v0.2.6.2) option using a minimum contig size of 2.5 kb, and CheckM (Parks et al., 2015) was used to assess bin quality. The 25 high- and medium-quality bins reported here (>50% completeness and <10% redundancy; Bowers et al. (2017)) represent 30%–35% of the total sequence coverage for each sample (Data Set S5). High-redundancy bins were broken up and optimized via visualization in anvi'o v6.2 (Eren et al., 2015).

The *Serpentinomonas* and *Truepera* MAGs described here were binned from the metagenomic data set reported by Seyler et al. (2020). Briefly, metagenomic sequencing was conducted at the Joint Genome Institute on an Illumina HiSeq2000 instrument with DNA sheared to 270-bp fragments using a Covaris LE220 ultrasonicator and SPRI magnetic beads (Rohland & Reich, 2012). Ten libraries were pooled per lane and prepared for sequencing. Co-assembly was performed with Ray Meta v.2.3.1 (Boisvert et al., 2012), and MAGs were binned with ABAWACA v.1.00 (https://github.com/CK7/abawaca) and refined with Binsanity.

All MAGs were further analyzed in KBase (Arkin et al., 2018), including taxonomic classification with GTDB-Tk (v1.1.0 using release 89 data; Chaumeil et al., 2019). GhostKOALA v2.2 was used to identify the completeness of metabolic pathways for each MAG (Kanehisa et al., 2016). The coverage of each contig was calculated as the total sequencing coverage of reads mapped to the contig by bowtie2, divided by the length of the contig to obtain an average coverage per position. Contig coverages were normalized to the total coverage for each library, multiplied by 10^6 for final units of transcripts (or fragments) per million (TPM). Because TPM is a proportional metric, unlike FPKM, it is considered to be more appropriate for comparisons of coverage among samples. The coverage of each MAG was calculated as the sum of the normalized, proportional coverages (in TPM) of its member contigs.

2.7. Phylogenetic Trees

Maximum likelihood phylogenetic trees were generated in ARB v.6.0.4 (Ludwig et al., 2004) for 16S rRNA gene sequence OTUs related to *Truepera*, *Serpentinomonas*, and *Dethiobacter* present at >0.1% abundance in the final data set. Using SILVA database v138, sequences for each tree and a relevant set of reference sequences were aligned in ARB to the *E. coli* reference sequence. For the *Serpentinomonas* tree, additional reference sequences included 16S rRNA gene sequences from the complete translated genome assemblies of *Serpentinomonas* isolates from The Cedars (Suzuki et al., 2014; *S. raichei* strain A1, *S. raichei* strain H1, and *S. mccroryi* strain B1; accession numbers MT882023.1, BAWN01000024.1 contig 24, and AP014569.1 respectively) from the NCBI database. After alignment, the shortest sequence was identified and longer sequences were trimmed to the same length (253 bp). Preliminary trees were created using AxML, before a final 1000-bootstrapped maximum likelihood tree was created using RAxML. Bootstrap values >50% are shown at branch nodes.

3. Results

3.1. CSW1.1 Water Column Chemistry and Energy Availability

The CSW1.1 well was drilled through complex subsurface lithologies to access a deep confined aquifer. The well was initially drilled to 31 m, but collapsed and is only accessible to 19.5 m (Ortiz et al., 2018). It is important to note that the well is cased down to 15 m, and the in situ well pump sits at 19.5 m, so part of CSW1.1 is uncased toward the base. As water was extracted from the potentiometric surface (topmost layers of water in the well), the water level decreased which lowered the hydraulic head and caused some recharge to occur between the 50% and 15% oxygen (O_2) sampling points. This placed the measured 15% O_2 sample (3.21 m) depth physically above the 50% sample (3.41 m). While this apparent recharge caused the measured potentiometric surface depth to be temporarily elevated, water still maintained an O_2 concentration of 15% ± 1% air saturation while all samples at this interval were taken.

As O_2 concentrations decreased through the well profile, the measured water chemistries also varied across the four depths (Figure 1; Table 1). Throughout the profile, pH stayed fairly consistent at 11.9 ± 0.1. Conductivity slightly increased toward the bottom of the well, and ORP generally dropped with depth, with a

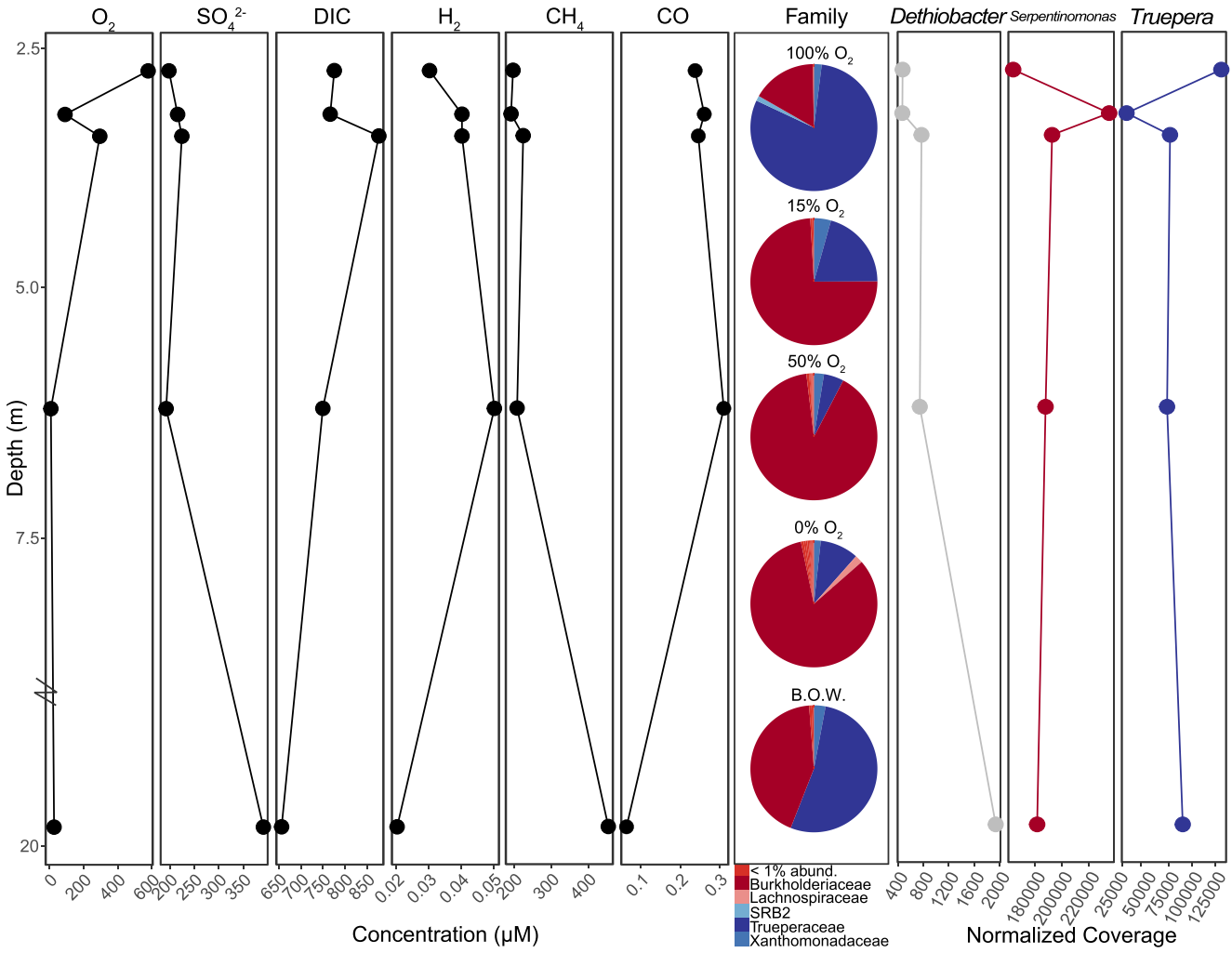

Figure 1. CSW1.1 depth profile and bottom of well water chemistry, 16S rRNA gene sequence data >1% abundance, and metagenome assembled genome normalized coverage in transcripts per million for *Dethiobacter*, *Serpentinomonas*, and *Truepera* bins.

slight increase at 15% O_2. Total HS^- remained low throughout the profile, but was detectable at 3.54 μM at the bottom of the well (BOW). SO_4^{2-} started at 197 μM, increased slightly toward the middle of the well profile, dropped off toward 0% O_2, and then increased to 390 μM at the BOW. NO_3^- and NO_2^- remained below detection throughout CSW1.1. H_2 had a consistent increase down the profile (0.03–0.05 μM), but decreased slightly at the well bottom to 0.02 μM. CO concentrations also increased down the profile (0.24–0.31 μM),

Table 1
Measured CSW1.1 Depth Profile and Well Bottom Water Chemistry

%Air sat	O_2	Depth	pH	T	ORP	Cond	HS^-	SO_4^{2-}	Cl^-	Br^-	NO_3^-	NO_2^-	DIC	H_2	CO	CH_4	Cells/mL
100%	287	2.81	12.0	15.0	−224	3,706	<1.00	197	3,382	1.40	<1.00	<1.00	774	0.03	0.24	194	4.70
50%	146	3.41	11.8	15.2	−228	3,738	<1.00	223	3,424	<1.00	<1.00	<1.00	875	0.04	0.24	222	3.08
15%	43.7	3.21	11.8	15.0	−214	3,667	<1.00	215	2,932	<1.00	<1.00	<1.00	765	0.04	0.26	189	3.37
0%	2.22	5.91	11.9	15.0	−227	3,778	<1.00	191	3,399	<1.00	<1.00	<1.00	748	0.05	0.31	205	2.64
3%	7.19	19.50	12.0	18.7	−262	3,820	3.54	390	2,466	30.9	<1.00	<1.00	655	0.02	0.06	452	6.66

Note. Concentrations in μM, except depth (m), T (ºC), ORP (mV), and conductivity (μS/cm)% air saturation = oxygen level relative to the concentration of atmospheric oxygen; Cells/mL values = $\times 10^5$.
Abbreviations: DIC, dissolved inorganic carbon; O_2, dissolved oxygen; ORP, oxidation-reduction potential.

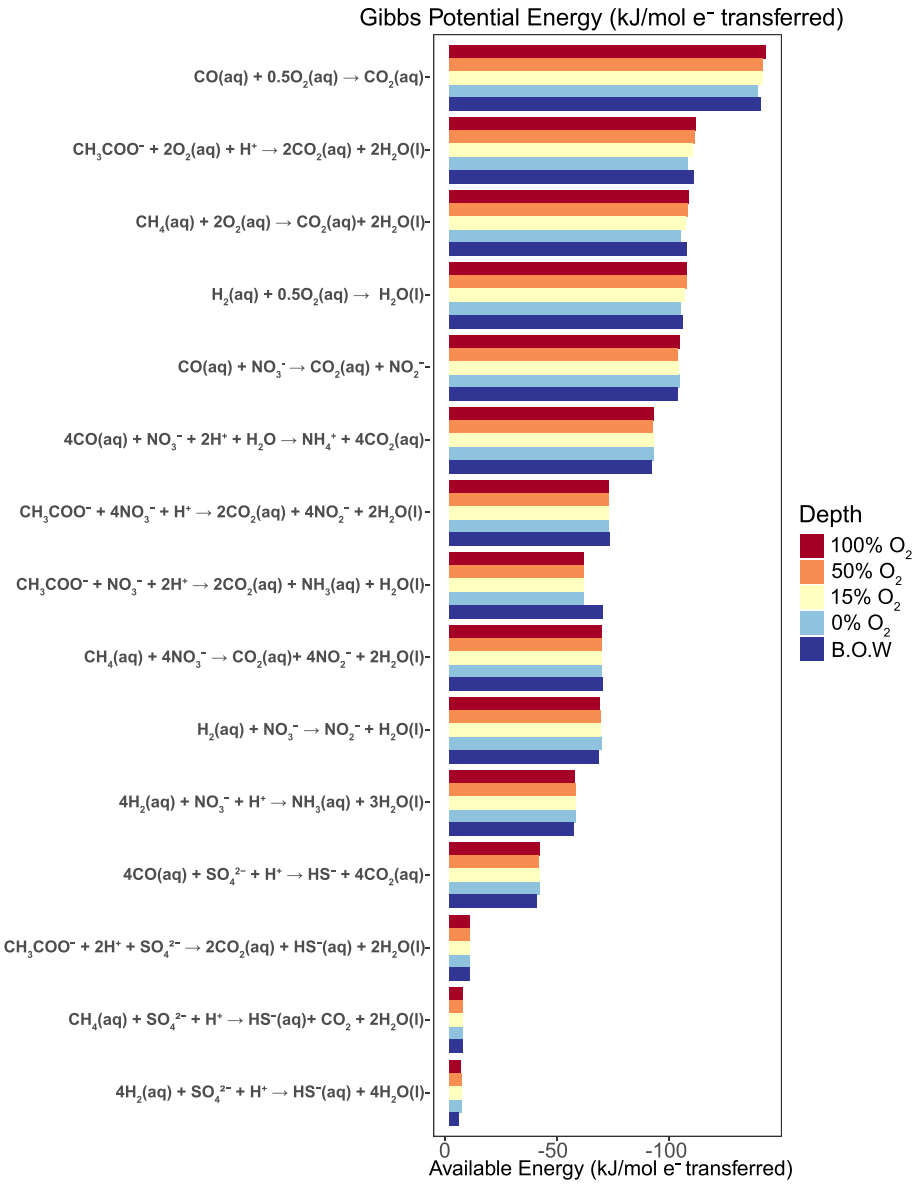

Figure 2. Gibbs energy (kJ/mol e^- transferred) calculated for each depth in the CSW1.1 profile and bottom of the well for a suite of redox reactions (Data Set S1). Full reactions for the abbreviated *y*-axis labels can be found in Table S1.

and dropped at the BOW to 0.06 μM. CH_4 concentrations oscillated around 200 μM in the profile before increasing to ~450 μM at the BOW (Figure 1; Table 1).

Gibbs energy for all reactions calculated provided a net energy yield above the −20 kJ/mol minimum needed to be considered biologically useful (Hoehler et al., 2001; Schink, 1997). When normalized to energy available in kJ/mol e^- transferred, reactions generally followed the classical electron tower profile. O_2 consuming reactions generated the most energy, followed by NO_3^- and then SO_4^{2-} (Figure 2). CO was the most energetically favorable electron donor, followed by acetate, CH_4, and H_2. The reactions were generally limited by the concentration of the electron donors, with the exception of CH_4, which is atypical of serpentinizing systems. When normalized per liter of groundwater, all electron acceptors when coupled to CH_4 as an electron donor provide considerably more energy than reactions involving CO and H_2 (Figure 3). If acetate (CH_3COO^-) is present at 1 μM as was estimated for these calculations, it would represent the second most abundant energy source and supply more energy than H_2 or CO. If acetate is higher, as measured in the CSW1.1 well at CROMO in previous studies (e.g., Crespo-Medina et al., 2014), it could play an even larger

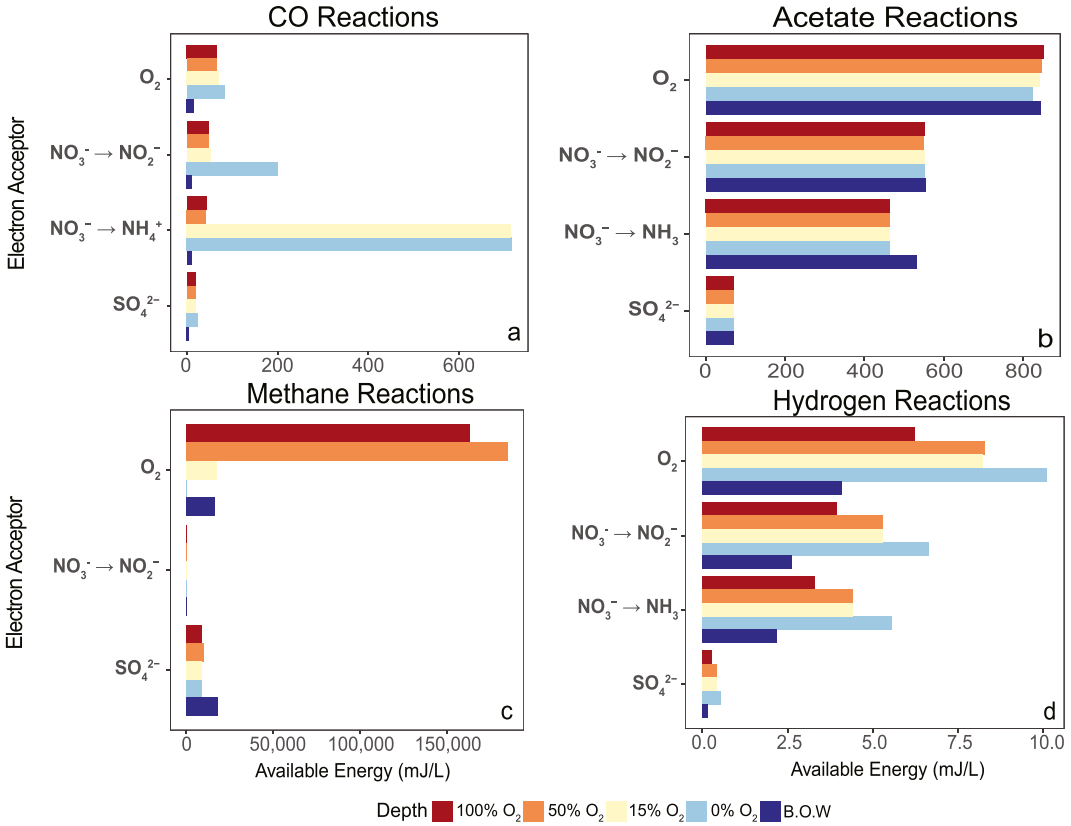

Figure 3. Gibbs energy normalized per liter of groundwater (volumetric energy; mJ/L) available at each depth in the CSW1.1 profile and bottom of the well for a suite of electron acceptors coupled to (a) carbon monoxide, (b) acetate, (c) methane, and (d) hydrogen (Data Set S1). Full reactions for the abbreviated *y*-axis labels can be found in Table S1 and numerical values are available in Data Set S2. Note the distinct *x*-axis scales for each panel.

role. The full reactions for Figure 3 can be found in Table S1. CH_4 would provide up to 185,000 mJ/L at the top of CSW1.1 when coupled to O_2 at the top of the profile, with yields decreasing as O_2 levels decreased in the well. In these reactions, CH_4 was the limiting reactant at 100% and 50% O_2, which quickly switched to O_2 as the limiting reactant with depth. CH_4 coupled to SO_4^{2-} increased in energy availability from ~8,700 to 18,000 mJ/L with depth, and generally sulfate was the limiting reactant. Acetate (the limiting reactant) coupled to O_2 provided ~800 mJ/L, ~500 mJ/L when coupled with NO_3^-, and ~100 mJ/L coupled to SO_4^{2-}. The exception to acetate or methane reactions providing the most energy is CO coupled to NO_3^- to produce ammonium (NH_4^+), where in this set of reactions the limiting reactant switched to NO_3^- and lower profile samples could provide >600 mJ/L of energy. Otherwise, CO reactions generally provided ~50–200 mJ/L and slightly increased in energy availability with depth. Reactions involving H_2 generally increased in energy availability with depth in CSW1.1 and according to the electron tower (Figures 2 and 3; Data Set S1).

3.2. Microbial Communities and Metabolic Pathways Present in CSW1.1

Bacterial communities throughout the CSW1.1 well had cell abundances on the order of 10^5 cells/mL. With increasing depth, cell abundances generally decreased, with the exception of the well bottom, where abundances increased slightly (Table 1). The families Trueperaceae and Burkholderiaceae (which include the genera *Truepera* and *Serpentinomonas,* respectively) were major components of the microbial communities in the well water, and Xanthomonadaceae was consistently found throughout the depth profile (Figure 1). In addition to these taxa, at the top of the well (100% O_2), SRB-2 (Thermoanaerobacterales) were also present. Deeper into the well, Trueperaceae generally decreased in abundance but Burkholderiaceae increased, and extended to 75% of the total microbial community at 0% O_2. At the CSW1.1 BOW, Trueperaceae and Burkholderiaceae each comprised ~48% of the community, while Xanthomonadaceae and

Table 2
Key Genes in CSW1.1 Depth Profile Metagenomic Data

Description	KEGG ID	Gene name	100% O_2	50% O_2	15% O_2	0% O_2	BOW
Cytochrome C oxidase	K02258	*COX, low affinity*	6.63	5.83	4.97	6.69	7.77
Oxygen Detoxification	K04564	*SOD*	322	273	232	286	280
Cytochrome C oxidase	K00404	*cbb3-type, high affinity*	165	211	258	212	213
Cytochrome bd complex	K00425	*cydA, high affinity*	314	372	460	399	383
Nitrate Reduction	K00370	*narG*	3645	3577	3658	3799	3647
Nitrite Reduction	K03385	*nrfA*	115	63.6	25.1	71.7	79.1
	K00362	*nirB*	883	1035	1265	1092	990
Sulfite Reduction	K11180	*dsrA*	0.00	0.00	0.00	0.08	0.09
Thiosulfate oxidation	K17226	*soxY*	156	174	194	187	165
	K17227	*soxZ*	75.3	74.8	94.8	87.0	72.8
CO oxidation (aerobic)	K03520	*coxL,cutL* (Mo)	84.0	116	170	104	99.1
CO oxidation (anaerobic)	K00198	*cooS* [NiFe]	1.06	1.23	0.73	1.62	4.25
Methane oxidation	K16157-62	*mmo*	absent				
	K10944-46	*pmo*	absent				
Hydrogen Oxidation Group 1	K06281	*hyaB* ([NiFe])	224	282	294	274	226
Group 3d	K18005	*hoxF* ([NiFe])	1453	1857	2259	1953	1920
Group 3d	K00436	*hoxH* ([NiFe])	1138	1108	1064	1142	1111
	K18331	*hndA* ([FeFe])	0.31	0.58	0.83	0.95	1.37
NADH Hydrogenase Complex	K00336	*nuoG* (Fe only)	1086	1092	1035	1112	1085
Carbon fixation genes	K01601	*cbbL* (CBB pathway)	1228	1463	1799	1554	1423
	K14138	*acsB* (Wood-Ljungdahl)	0.95	2.96	0.55	1.70	5.05
	K01938	*fhs* (Wood-Ljungdahl)	559	333	121	351	390
Heterotrophy	K00240	*sdhB* (TCA cycle)	890	793	655	830	777
	K00031	*icd* (TCA cycle)	7773	7871	8576	8085	7851
	K00128	ALDH (Glycolysis)	2799	2221	1965	2209	2347
	K00849	*galK* (Glycolysis)	500	326	96.2	307	317

Note. Gene abundances are reported here in metagenome fragments per kilobase of predicted protein sequence per million mapped reads (FPKM). Numbers highlighted in red show the lowest gene abundance in the row, and blue highlighted values show the highest value in the row.

organisms present at <1% abundance comprised the remaining 2% (Figure 1). Of the total 16S rRNA gene data set, only 11 OTUs were present at > 0.01% relative abundance (Table S2). The closest relatives of these OTUs were identified as *Serpentinomonas raichei* strain A1, *Truepera radiovictrix, Dethiobacter alkaliphilus, Methylobacterium bullatum, Gracilibacter thermotolerans*, and *Hydrogenophaga soli* (6 OTUs). *S. raichei* and *M. bullatum*-like populations were most abundant in the middle of the profile, whereas *T. radiovictrix*-like populations were most abundant at the top of the profile. *D. alkaliphilus* peaked at the base of the well, and *H. soli* was fairly ubiquitous throughout CSW1.1 (Table S2).

Phylogenetic trees for *Serpentinomonas* (Figure S2), *Truepera* (Figure S3) and *Dethiobacter* (Figure S4) were used to visualize the relationship between each of these dominant populations, including CROMO OTUs present in >0.1% abundance, and a set of closely related reference organisms. Two OTUs (OTU 26671 and OTU 96041) branched tightly with *S. raichei* strain A1. The tree created for OTUs closely matching *Truepera* showed 21 OTUs branched from *T. radiovictrix* (listed in Figure S3 caption). One OTU (OTU 237261) matched closely with *D. alkaliphilus* AHT1.

Metagenomes constructed from groundwater at various depths in the CSW1.1 profile and well bottom revealed a variety of key genes involved in the consumption of dissolved gases, including H_2, CO, and O_2. Genes for hydrogen oxidation included those from Groups 1 and 3d hydrogenases, such as *hyaB* (hydrogenase large subunit) and *hoxH* and *hoxF* ([NiFe]-hydrogenases; NAD-reducing hydrogenase large subunit; bidirectional [NiFe] hydrogenase diaphorase subunit) respectively (Table 2). These genes were most abundant near the oxic-anoxic interface, where *hyaB* and *hoxF* peaked at 15% O_2 (294 FPKM; 2259 FPKM respectively), and *hoxH* peaked at 0% O_2 (1143 FPKM), and are consistent with the concept of H_2 consumption. The gene complex *hndABCD* ([FeFe]-hydrogenase) was also present in lower quantities, with a peak in abundance at the well base (0.31 FPKM low at 100% O_2; 1.37 FPKM peak at the well base). For a more

detailed description of hydrogenase groups and their roles, see Data Set S6, Søndergaard et al. (2016), and reviews by Greening et al. (2016) and Peters et al. (2015). Genes for aerobic and anaerobic carbon monoxide oxidation were present throughout CSW1.1. The aerobic CO oxidation gene *coxL* (aerobic carbon-monoxide dehydrogenase large subunit) peaked in abundance at 15% O_2 (170 FPKM), whereas the anaerobic *cooS* gene (anaerobic carbon-monoxide dehydrogenase catalytic subunit) peaked at the well base (4.25 FPKM). Genes for high and low affinity cytochromes were detected in the well, which are associated with oxygen respiration under microaerophilic and aerobic conditions, respectively. High affinity cytochromes, including cytochrome C oxidase represented by cbb3-type cytochromes and cytochrome bd complex represented by *cydA*, were most abundant at the oxic-anoxic interface (15% O_2; 258 FPKM and 460 FPKM respectively) and lowest at the top of the well profile (100% O_2; 165 FPKM and 314 FPKM respectively). Low affinity cytochrome c oxidase, represented by COX, was not very abundant overall, but was slightly more so at the well bottom (7.77 FPKM) than near the oxic-anoxic interface (15% O_2; 4.97 FPKM). Oxygen detoxification enzymes present included superoxide dismutase (SOD), which was most abundant at the top of the profile (100% O_2; 322 FPKM) and least abundant at the oxic-anoxic interface (15% O_2; 232 FPKM). Notably absent throughout CSW1.1 were genes for aerobic methane oxidation (*mmoXYZ*, *mmoCBD*, *pmoABC*) and genes responsible for biological methanogenesis or the anaerobic oxidation of methane such as *mcrA* (Table 2; Data Set S4).

Carbon assimilation pathways particularly abundant in CSW1.1 included genes for carbon fixation (CBB cycle) and heterotrophy (citrate cycle, glycolysis, and pentose phosphate pathway). A key gene in the CBB cycle, *cbbL* (Rubisco large subunit gene), peaked in abundance at 15% O_2 (1799 FPKM) and was lowest at the top of the profile (100% O_2; 1228 FPKM). Genes for the reductive acetyl-CoA pathway (Wood-Ljungdahl) were also present (Table 2). Though they varied in abundance throughout the well, the representative gene *acsB* (part of Wood-Ljungdahl; acetyl-CoA synthase) was most abundant at the well base (5.04 FPKM) and dipped to 0.55 FPKM toward the oxic-anoxic interface (15% O_2). Formate tetrahydrofolate ligase (*fhs*; part of Wood-Ljungdahl and also relevant for C1 interconversions) peaked at 100% O_2 (559 FPKM) and was lowest at 15% O_2 (121 FPKM). Succinate dehydrogenase (*sdhB*), a key gene of the tricarboxylic acid cycle (TCA cycle), peaked at the top of the profile (100% O_2; 890 FPKM) and was another gene to drop off near the oxic-anoxic interface at 15% O_2 (655 FPKM). Key genes for glycolysis (heterotrophy), *galK* (galactokinase) and ALDH (aldehyde dehydrogenase), varied throughout the well column but peaked at 100% O_2 (500 FPKM; 2799 FPKM respectively) and dropped off to a low at 15% O_2 (96.2 FPKM; 1965 FPKM respectively; Table 2).

In addition to the apparent importance of oxidative respiration and carbon transformations, the presence of key genes for nitrogen and sulfur cycling highlights the potential importance of metabolisms involving these compounds. A representative gene for dissimilatory nitrate reduction, *narG* (nitrate reductase), peaked in abundance at 0% O_2 (3799 FPKM), and stayed relatively consistent throughout the profile; the lowest abundance of *narG* was at 50% O_2 (3577 FPKM). Genes representative of nitrite reduction included *nrfA* (nitrite reductase) and *nirB* (nitrite reductase (NADH) large subunit), were both abundant throughout the well profile, but followed different trends. The *nrfA* gene was most abundant at 100% O_2 (115 FPKM), and lowest at 15% O_2 (25.1 FPKM), while the *nirB* gene peaked at 15% O_2 (1265 FPKM) and dropped to a low at 100% O_2 (883 FPKM). Gene *nirK* encoding NO-forming nitrite reductase was most abundant at 100% O_2 (636 FPKM) and lowest at 15% O_2 (25.1 FPKM; Data Set S4), but *nirS* (another NO-forming nitrite reductase gene) was not present in the data set. Genes for sulfate reduction, including dissimilatory sulfite reductase *dsrAB,* were not detected in the profile except for a small quantity toward the well base (~0.08 FPKM). Additionally genes for thiosulfate oxidation (SOX enzyme complex) were present, but only included *soxYZ*. These thiosulfate oxidation genes both peaked at the oxic-anoxic interface at 15% O_2 (194 FPKM *soxY*; 94.8 FPKM *soxZ*) (Table 2).

To investigate the metabolic capabilities of the most abundant organisms in the CSW1.1 profile, three MAG bins previously published in Seyler et al., (2020) related to *Serpentinomonas* (bins 66, 119, and 123) and two bins related to *Truepera* were examined here (bins 191, 207; Figures 4a and 4b). *Serpentinomonas* bins 119 and 123 had a completeness of 60% and 55% and contamination of 0% and 0.2% respectively. For *Truepera*, bins 191 and 207 had a completeness of 89% and 59% and contamination of 6% and 2% respectively (Table S2 from Seyler et al., 2020). CSW1.1 *Truepera* MAG bins were compared to reference organisms *Truepera radiovictrix, Deinococcus deserti, Deinococcus geothermalis, Deinococcus maricopensis,* and *Meiothermus*

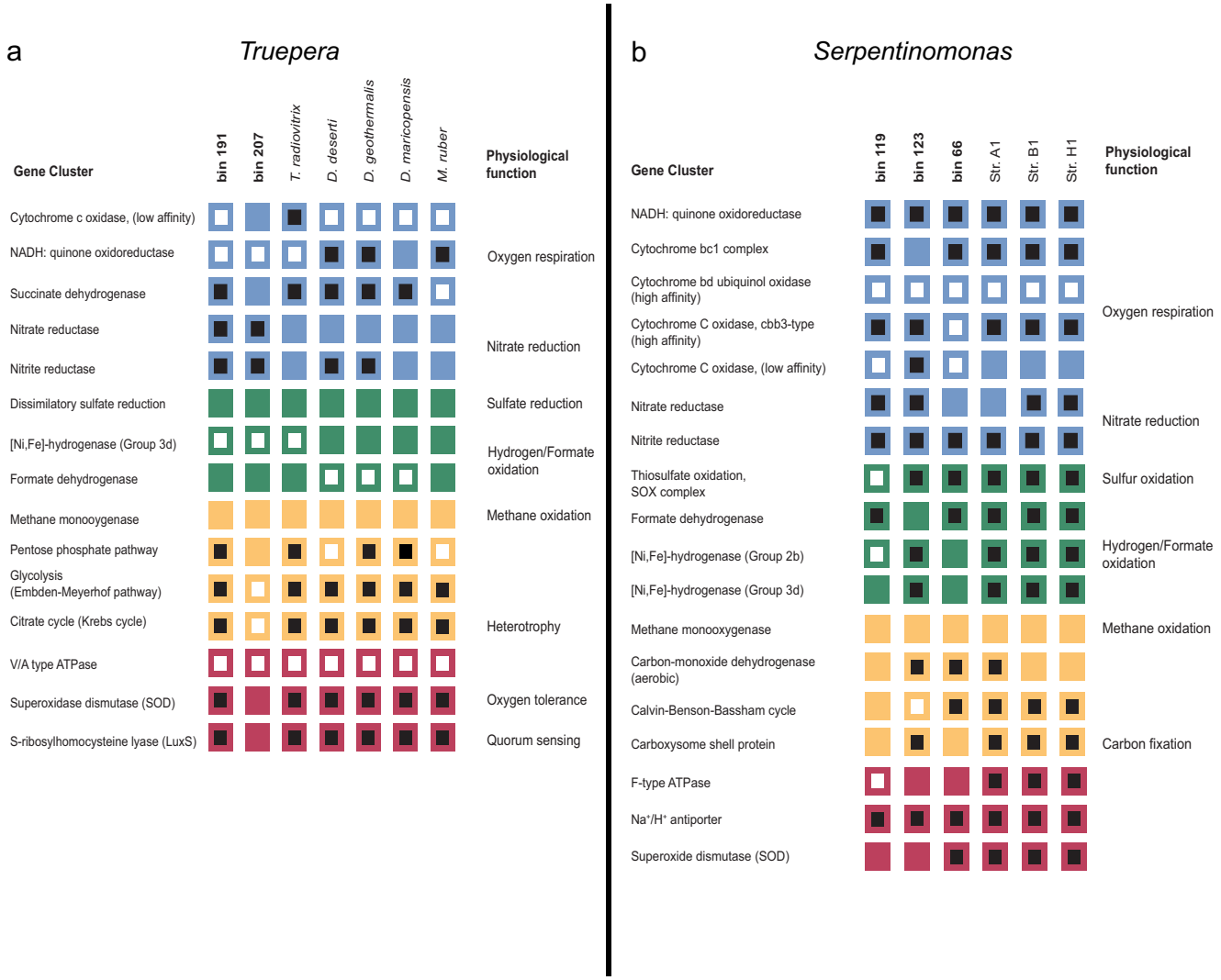

Figure 4. Box diagram of select metabolic pathway presence in metagenome assembled genome bins closely related to (a) *Truepera*, (b) *Serpentinomonas*, and respective reference organisms, modeled after Suzuki et al. (2014). Black squares indicate a gene or gene cluster is present in the respective bin or genome, whereas white squares indicate only one gene is missing from a cluster. Those without white or black squares (i.e., solid color squares) indicate two or more genes are missing from the pathway.

ruber. Both *Truepera* CROMO bins show complete pathways for nitrate and nitrite reduction, and *D. deserti* and *D. geothermalis* also have the nitrite reductase gene. Bin 191 and all reference organisms have the succinate dehydrogenase gene. Both bins and *T. radiovictrix* possess group 3d [NiFe]-hydrogenases, but neither of the bins have the formate dehydrogenase gene that *D. deserti, D. geothermalis,* and *D. maricopensis* have. All bins and reference organisms have the genes for glycolysis and heterotrophic carbon assimilation via the citrate cycle pathway. Bin 191 and all reference organisms possess genes for the pentose phosphate pathway and SOD (Figure 4).

The *Serpentinomonas* bins were compared to the previously published genomes of *Serpentinomonas raichei* strain A1, *Serpentinomonas raichei* strain H1, and *Serpentinomonas mccroryi* strain B1 (Suzuki et al., 2014). Overall, CSW1.1 *Serpentinomonas* bins are quite similar to the reference organisms, with a few differences scattered throughout. Bins 119 and 123 have complete pathways for nitrate and nitrite reductases similar to the three reference organisms, but bin 66 lacks the nitrate reductase gene. All have some of the genes for thiosulfate oxidation via the SOX complex, sodium-hydrogen antiporters, and only bin 123 is missing the gene encoding formate dehydrogenase. Bin 123 and the three reference strains contain the carboxysome shell protein, which is associated with the organelle where carbon dioxide is concentrated and carbon

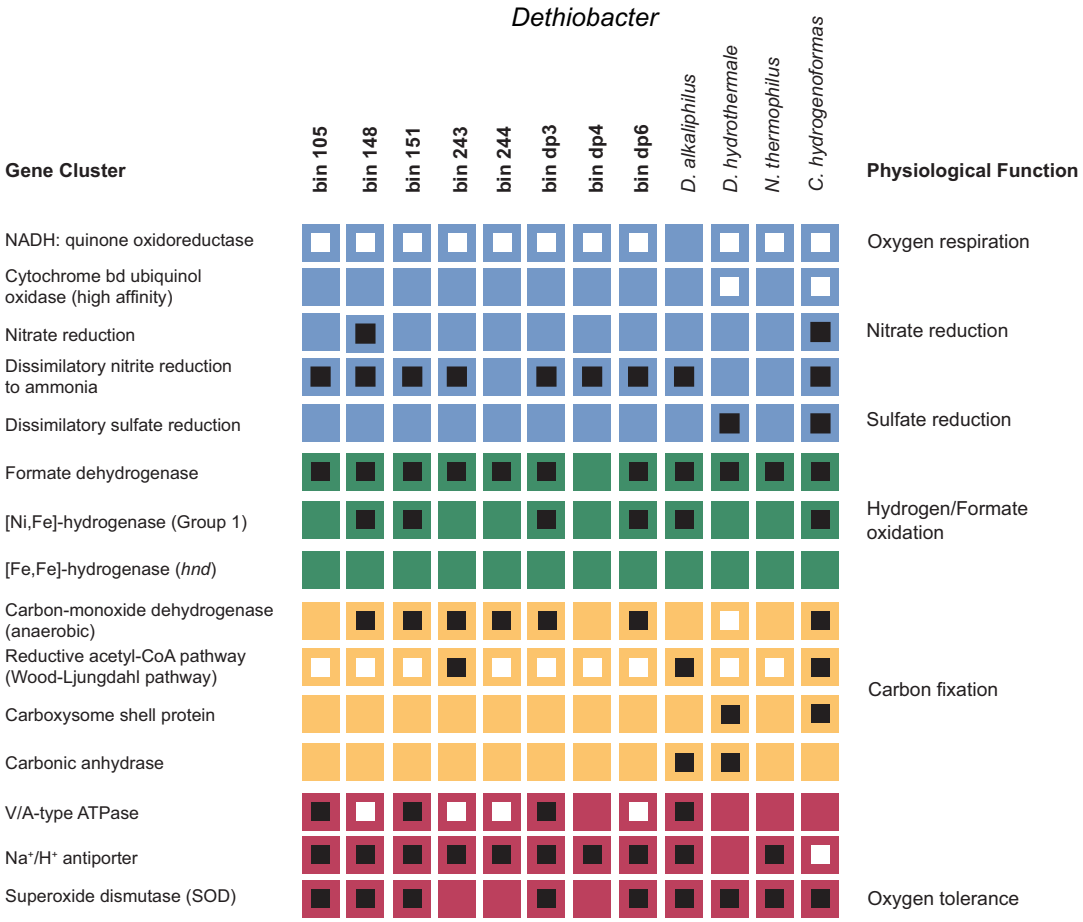

Figure 5. Box diagram of select metabolic pathway presence in metagenome assembled genome bins closely related to *Dethiobacter*, and respective reference organisms, modeled after Suzuki et al. (2014). Black squares indicate a gene or gene cluster is present in the respective bin or genome, whereas white squares indicate only one gene is missing from a cluster. Those without white or black squares (i.e., solid color squares) indicate two or more genes are missing from the pathway.

fixation takes place. Carbon monoxide dehydrogenase (aerobic) is present in bin 123 and 66, and is also in *S. raichei* strain A1. Bin 66 contains SOD along with all three reference strains.

High completion MAG bins created from the depth profile metagenomic data included a few that closely matched *Dethiobacter* (bins dp3, dp4, and dp6). Depth profile bin dp3 had 93% completeness and 1.4% contamination, dp4 had 93% completeness and 1% contamination, and dp6 had 91% completeness and 1.1% contamination. These bins were compared to MAG bins from Seyler et al. (2020) (bins 105, 148, 151, 243, 244) and complete genomes of *Dethiobacter alkaliphilus, Desulfotomaculum hydrothermale, Natranaerobius thermophilus,* and *Carboxydothermus hydrogenoformans* (Figure 5). *Dethiobacter* bins 105–244 ranged in completion from 54%–94%, and 1.5%–4.3% contamination (Seyler et al., 2020). CSW1.1 *Dethiobacter* bins did not match perfectly with any of these reference organisms, but did share similarities to all four. Only bin 148 and *C. hydrogenoformans* contained the nitrate reduction gene. All CSW1.1 *Dethiobacter* bins except bin 244 included complete pathways for DNRA, and all except bin dp4 contained formate dehydrogenase. No CROMO bins contained dissimilatory sulfate reduction genes, but reference genomes *D. hydrothermale* and *C. hydrogenoformans* did. [NiFe]-hydrogenase (group 1) was present in bin 148, 151, dp3 and dp6, as well as *D. alkaliphilus* and *C. hydrogenoformans*. The anaerobic version of carbon monoxide dehydrogenase was present in all bins except bin 105 and dp4. It was also present in *D. hydrothermale* and *C. hydrogenoformans*. The reductive acetyl-CoA pathway (Wood-Ljungdahl) was present to some extent in all bins and reference organisms, and oxygen tolerance genes (i.e., SOD) was present in all except bin 243, 244, and dp4 (Figure 5).

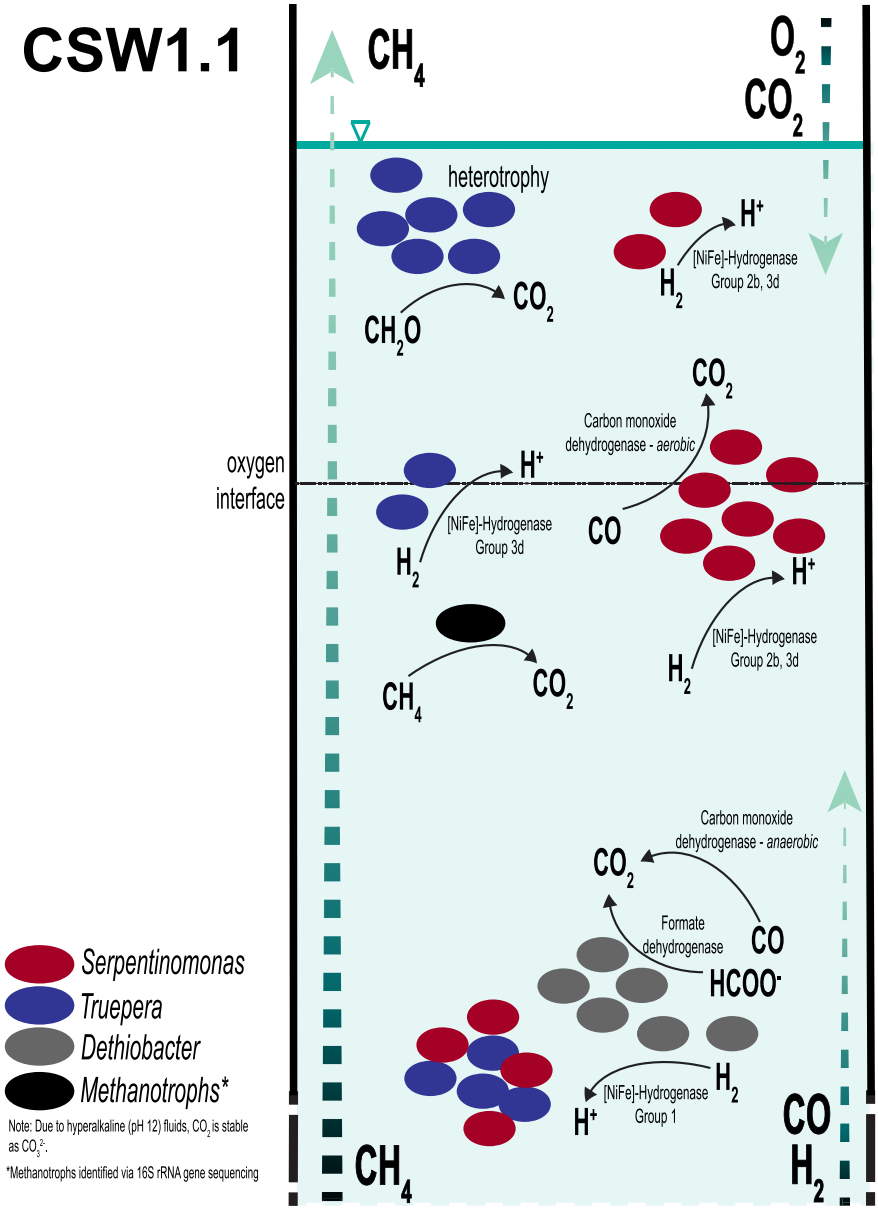

Figure 6. Conceptual diagram of atmospheric (O_2, CO_2) and serpentinization-related inputs (CO, H_2, CH_4) to CSW1.1 well fluids coupled with metabolic pathways associated with *Serpentinomonas*, *Truepera*, and *Dethiobacter* metagenome assembled genomes with depth.

With this information, a conceptual diagram was created to visualize the relationships between these dominant genera and model the biogeochemical interactions occurring (Figure 6).

In these three dominant genera present in CSW1.1, all had at least one bin with nitrate and nitrite reductase. *Serpentinomonas* and *Dethiobacter* bins contained genes for formate dehydrogenase, whereas *Truepera* did not. All organisms had some version of a [NiFe]-hydrogenase present, but *Truepera* had group 3d, *Serpentinomonas* had group 2b and 3d, and *Dethiobacter* possessed group 1. *Serpentinomonas* bins contained the aerobic carbon monoxide dehydrogenase while *Dethiobacter* had the anaerobic version. All three genera had at least one bin for SOD to handle oxidative stress (Figures 4 and 5).

4. Discussion

The extreme ultrabasic and reducing conditions generated through serpentinization create chemical conditions that are very distinct from those characteristic of surface and near-surface groundwaters. Mixing between these fluids can create steep chemical gradients in the subsurface. Characterizing the microbiology and geochemistry of these gradients *in situ* provides important insight into how resident microbial communities both benefit from and shape this geochemical setting. Through the window provided by monitoring wells at CROMO, including CSW1.1, CH_4, H_2, and CO gases generated directly and indirectly by serpentinization diffuse up from the subsurface and can be used as fuel by microbial communities or escape to the atmosphere (McCollom & Seewald, 2013). Similarly, atmospheric CO_2 and O_2 diffuse downward into the subsurface, where they are then transformed or consumed. The concentration of available electron acceptors such as O_2, NO_3^-, SO_4^{2-} are generally limited in serpentinizing systems (Fones et al., 2019; McCollom & Seewald, 2013; Rempfert et al., 2017; Schrenk et al., 2013). Due to the characteristically high pH fluids generated by this process, DIC is also scarce, as it is sequestered into carbonate minerals. This imposes unique challenges for life in serpentinites relative to habitats at the Earth's surface. Organisms such as the candidate genus *"Serpentinomonas"* (Burkholderiales) are adapted to thrive in these waters, utilizing a range of carbon and energy sources (Suzuki et al., 2014). Here, we conducted a comprehensive profile across distinct depths in a serpentinization-influenced well to document biogeochemical processes occurring at a fine scale, and to consider their consequences for gas exchange with the surface and atmosphere.

4.1. Biogeochemical Gradients Fuel the Dominant Organisms in CSW1.1

The base of the CSW1.1 well provided a window into a deeper, more extreme system, as lithologies transitioned to more intact serpentine bedrock (Ortiz et al., 2018), and pH reached a site-wide May 2016 maximum of 12.0. At the well base, water chemistries exhibited higher conductivities and dissolved oxygen concentrations were around 3% of O_2 air saturation. This apparent presence of oxygen may be due to a discrepancy between detection limits in the DO probes used (ultrasensitive DO probe at top, YSI probe at bottom) or could be explained by mixing instigated by top-down movement of water through the uncased portions of CSW1.1 toward the hydraulic gradient generated by the pump sitting at the well base (Jones & Lerner, 1995). The latter would be consistent with the presence of some O_2-utilizing taxa near the well base.

At the bottom of CSW1.1, 16S rRNA gene sequence data indicated that organisms were divided almost evenly between two families, Trueperaceae (Truepera) and Burkholderiaceae (Betaproteobacteria). Trueperaceae, a family isolated from hot spring runoff in the Azores, contains the alkaliphilic and facultatively halophilic *T. radiovictrix* species capable of extreme radiation resistance (Albuquerque et al., 2005). This organism is related to the Deinococcus phylum (previously identified at the Prony Hydrothermal Field and Hakuba Happo hot springs, among others; Quéméneur et al., 2014; Merino et al., 2020) which includes the genus, *Meiothermus*, previously identified in high abundance at the Samail ophiolite in Oman (Rempfert et al., 2017). A closely related organism, *Deinococcus geothermalis*, was shown to grow in biofilms and channel central carbon metabolic pathways to modulate exposure to oxygen, and contains a similar biochemical repertoire seen in the Truepera MAGs at CROMO (Liedert et al., 2012). In *D. geothermalis*, SOD, the oxygen detoxification enzyme is key to combating oxidative stress and enhancing survival (Liedert et al., 2012). Examination of the MAGs (bin 191, bin 207) identified taxonomically as Truepera, reveals that they also possess nitrate and nitrite reductase genes involved in the DNRA. Further, while bin 207 is missing one gene from the pathway for the citrate cycle (Krebs cycle) and glycolysis, and more than one gene for the pentose phosphate pathway, bin 191 hosts the capability to perform heterotrophic carbon assimilation through complete pathways for the citrate cycle and the pentose phosphate pathway (Figure 4).

The Xanthomonadaceae family comprised the remaining few percent of the community >1%, and the top 11 OTUs >0.1% in this system included *D. alkaliphilus*, among others. *Dethiobacter* populations appeared near the oxic-anoxic interface, but peaked at the well base (Table S2). The *Dethiobacter* MAG bins from CROMO contain the complete pathway for DNRA (all bins except bin 244) but none had the ability to reduce sulfate. All bins except dp4 contained the formate dehydrogenase gene, and all possessed the anaerobic version of CO dehydrogenase (except 105 and dp4). The V/A-type ATPase (all bins except dp4), and Na^+/H^+ antiporter

(all 8 bins) play a role in high pH adaptation. This Na^+/H^+ antiporter likely regulates cytoplasmic pH and sodium homeostasis in cells, which is critical for survival in these ultrabasic environments.

It is important to note that 4 L of fluids were filtered for samples at the bottom of the well for 16S rRNA gene sequencing (compared to 400 mL per sample at the well top) due to the pre-installed bladder pump at the well base. While lower abundance organisms may have been missed from the top of the well, this was the only feasible way to extract fluid from the well without substantially disturbing the water column. However, the bulk community composition of organisms between the top and bottom of the well do not vary substantially. To this end, the community richness (Shannon Index) in the profile was similarly low at 100% O_2 and the well base, though it did increase toward the oxic-anoxic interface (Figure S5a). The community evenness in CSW1.1 profile samples was relatively consistent throughout (Figure S5b).

Throughout the more oxic portions of the CSW1.1 profile, an abundance of CH_4 (~200 μM), SO_4^{2-} (~200 μM), and DIC (~800 μM) was detected, with lower levels of CO (~0.25 μM), H_2 (~0.03 μM), and NO_3^- (~1 μM) and NO_2^- (~1 μM; Table 1). Total HS^- remained below detection limits in the profile due to the oxic conditions at the top of the well, but did increase at the well base to ~3 μM. Microbial sulfide oxidation processes can still take place below the detection limits of methods used here so processes involving sulfide could still occur (e.g., a more cryptic sulfur cycle; Kappler & Bryce, 2017). Community compositions indicated a dominance of only a few families throughout, and metagenomic data indicated an abundance of genes related to the transformation of carbon, sulfur, and nitrogen compounds.

Above the well base at 0%–50% O_2 levels, 16S rRNA gene sequence data showed that Burkholderiaceae become the dominant family. From previous studies, it was shown that Betaproteobacteria dominated serpentinite springs (Brazelton et al., 2012, 2013; Schrenk et al., 2013). Within this group, Burkholderiales inhabit oxygen-mixing zones and harbor the 3 known strains within the *Serpentinomonas* genus, which utilize H_2, calcium carbonate, and O_2 to generate energy (Suzuki et al., 2014). Two of the three strains (B1 and H1) are capable of nitrate reduction, but none is capable of sulfate reduction (Suzuki et al., 2014). Organisms related to *Serpentinomonas* have been identified previously in the high pH wells at CROMO (Twing et al., 2017), and are also identified here. *Serpentinomonas* is most abundant halfway through the profile at the oxygen interface where MAG bins 119, 123, and 66 possess multiple cytochromes for oxygen tolerance, including cytochrome bc1 complex (bin 119 and 66), cytochrome bd ubiquinol oxidase (high affinity; all 3 bins), cytochrome C oxidase cbb3-type (high affinity; all 3 bins), and cytochrome C oxidase (low affinity; all 3 bins; Figure 4). The *Serpentinomonas* MAG bins also contain pathways for nitrate reduction (bin 119, 123) and nitrite reduction (all 3 bins), and thiosulfate oxidation via SOX (all 3 bins). *Serpentinomonas* MAGs also encode the ability to oxidize hydrogen via group 2b and 3d [NiFe]-hydrogenases (bin 119 (2b) and 123 (2b, 3d)), and to aerobically transform carbon monoxide via CO dehydrogenase (bins 123 and 66). Finally, the bins contain the genes necessary for carbon fixation via the CBB cycle (reductive pentose phosphate pathway; bins 123 and 66). At 100% O_2, Trueperaceae was by far the most predominant family as identified by 16S rRNA gene sequence data, followed by Burkholderiaceae, SRB2 (Firmicutes), and Xanthomonadaceae (Gammaproteobacteria; Figure 1). Here at the top of the well, Trueperaceae are equipped to employ the use of biofilms or SOD to enhance survival in these higher O_2 waters. When combined, this biogeochemical profile reveals how organisms within the CSW1.1 well are fueled and equipped to survive.

4.2. Methane Reactions Provide the Greatest Available Energy, but Metagenomic Evidence for Methane Metabolism is Scarce

Microorganisms have been previously shown to use CH_4 through both aerobic (e.g., Kraus et al., 2021) and anaerobic oxidation of methane (AOM) coupled to sulfate, ferric iron, or manganese reduction (Beal et al., 2009; Orphan et al., 2002; Sivan et al., 2011). Chemosynthetic bacteria and archaea in seafloor hydrothermal systems have been shown to take advantage of the H_2 and CH_4 rich fluids and thermodynamic disequilibrium that results from the mixing of fluids (Brazelton et al., 2006). In the high pH and salinity fluids of Mono Lake, California, biological anaerobic methane oxidation was shown to be the primary sink for methane (Joye et al., 1999). Interestingly, no genes related to aerobic or anaerobic methane oxidation are detectable in CSW1.1 fluids here, despite the considerable Gibbs energy available for these processes (Figure 3; Table 2). Additionally, due to a consistent lack of evidence for biological methanogenesis at CROMO in this study and in previous studies (i.e., Twing et al., 2017), Gibbs energy for methanogenesis reactions

were not calculated. There is always the possibility that the relatively smaller sample volumes collected and analyzed in this study may have missed some less-abundant populations. At the top of the well, for example, CH_4 coupled to O_2 provides >150,000 mJ/L energy. This is similar to a study of deeply seated (>250–350m) groundwater in the Fennoscandian Shield below the island of Olkiluoto, Finland which showed no evidence for methane as an electron donor for microbially mediated sulfate reduction in the mixing zone between shallower sulfide-rich water and deeper methane-rich water (Bell et al., 2018). The ultrabasic fluids here could be challenging for organisms capable of transforming CH_4 due to the scarcity of H^+ ions available for the electron transport chain although methanotrophs and methanogens have been identified in high pH Mono Lake waters and serpentinizing systems such as the Samail ophiolite in Oman (Kraus et al., 2021).

Upon closer inspection of the organisms identified by 16S rRNA gene sequencing in CSW1.1, and those potentially involved in transforming methane, in the top 11 OTUs of the profile, *Methylobacterium bullatum* (Beijerinckiaceae) is present at >0.01% abundance (0.7% abundant; Table S2). *M. bullatum* is a strictly aerobic, motile, biofilm-producing, methane oxidizing bacterium (Hoppe et al., 2011). Of the organisms present at <1% abundance, *Methylobacter, Methylocystis,* and *Methylomonas* are also present (Table S2; Data Set S2; Bowman et al., 1993; Brazelton et al., 2006; Crespo-Medina et al., 2017; van Grinsven et al., 2020). These organisms are known aerobic methanotrophs, and inhabit oxic-anoxic transition zones (van Grinsven et al., 2020). At 100% O_2, only a few counts of *Methylomonas* were present. However, at 50% O_2, *Methylobacter, Methylocystis,* and *Methylomonas* are detected at a few counts each, and the *M. bullatum* population substantially increased to ~500 counts (Data Set S2). Evidence for methane oxidation has been recently identified in metatranscriptomes from CROMO well fluids, especially QV1.2 and N08-B (pH 9.3 and 10.2 respectively; Seyler et al., 2020). For these two wells in particular, metatranscriptome abundance (FPKM) for a particular gene, such as *pmoA, pmoB,* or *pmoC* was greater than the metagenomic abundance. However, while some evidence for methane oxidation was detected in metagenomic data for CSW1.1, all were <1 FPKM, which is extremely low (Table S1 of Seyler et al., 2020). The lack of transcriptomic and extremely minimal metagenomic evidence points against prolific methane oxidation in CSW1.1, but does not preclude the possibility of methane oxidation here or at other CROMO sites.

Genes involved with biological methanogenesis or AOM, such as *mcrA*, were undetectable throughout the profile. While the lack of detectable genes for methanogenesis and methanotrophy is consistent with previous CROMO work (i.e., Twing et al., 2017), in this higher-resolution profile where it was necessary to collect < 1L of fluid per sample to avoid disturbing the profile, the lack of these genes detected could also be due to an undersampling of rarer taxa (e.g., Fones et al., 2019). It is unknown whether these populations, represented by relatively few counts in the 16S rRNA gene sequence data are contributing to detectable bulk geochemical measurements made here. In future studies, metatranscriptomic data would be beneficial to directly assess the microbial activity at each depth in the profile.

4.3. Carbon Monoxide, Hydrogen, and Nitrate Metabolic Pathways Are Abundant in the Depth Profile

Interestingly, metabolic pathways involving CO, H_2, and NO_3^- appear to be abundant throughout the CSW1.1 profile, despite the low concentrations of these compounds and less energy available per liter of groundwater relative to methane oxidation reactions (Table 2; Figure 3). For example, CH_4 oxidation coupled to SO_4^{2-} reduction provides 8,500–20,000 mJ/L, whereas CO oxidation coupled to O_2 reduction provides only 15–85 mJ/L (Data Set S1). If production and consumption of the latter are closely coupled, the low energy values calculated here could be masking a higher energy flux and keeping the measured concentrations low. As described above, no genes for CH_4 transformations were identified in CSW1.1, but aerobic CO oxidation is detected in *Serpentinomonas* at the top of the well. From the standpoint of electron donors, CO can also be transformed anaerobically by *Dethiobacter* near the base as part of the Wood-Ljungdahl pathway (Figure 4).

H_2 metabolisms have also been identified in serpentinizing systems at the Lost City Hydrothermal Field and the Tablelands ophiolite in Newfoundland, Canada, where novel [NiFe]-hydrogenases for H_2 oxidation were linked to Burkholderiales and H_2 production was generated by Clostridiales via [FeFe]-hydrogenases (Brazelton et al., 2012). Recent work described the presence of different [NiFe]-hydrogenases in Oman's Samail ophiolite (Fones et al., 2020). At CROMO, H_2 can be oxidized by all three organisms through

[NiFe]-hydrogenases (*Serpentinomonas* - Group 3d and 2b, *Truepera* Group 3d, and *Dethiobacter* Group 1). Table S1 by Seyler et al. (2020) describes metagenome and metatranscriptome data at the CROMO site and shows *hyaA* and *hyaB* ([NiFe]-hydrogenase large and small subunits) are active in wells that were sampled for metatranscriptome activity (wells QV1.1, QV1.2, N08-B, and CSWold). Another [NiFe]-hydrogenase small subunit encoded by *hydA* was detected in N08-B and QV1.2. Metatranscriptome data in that study showed a range of values from 6.31 FPKM in QV1.1 to 948 FPKM in CSWold. While CSW1.1 has not been sampled for gene expression yet, measured H_2 concentrations (Table S3) from that same study show CSW1.1 H_2 levels are slightly higher than the other wells with reported hydrogenase activity, and thus should be sufficient to support at least some hydrogenase activity. The prevalence of pathways for H_2 consumption across the entirety of the depth profile likely contributes to the depletion of these gases before reaching the surface.

Work by Canovas et al. (2017) at the Samail ophiolite indicated that microbial metabolism could be supported by reactions involving nitrogen compounds such as ammonia (NH_3) oxidation or NO_2^- oxidation coupled to O_2 reduction, N_2 reduction coupled to H_2 oxidation, NO_3^- reduction coupled to H_2 oxidation, and NO_2^- reduction coupled to NH_3 oxidation (anammox). Rempfert et al. (2017) identified the presence of nitrifiers, such as organisms in the Nitrososphaeraceae family within the archeal Thaumarchaeota phylum and members of the *Nitrospira* genus within the Nitrospirales order. In CSW1.1 groundwater, DNRA potentially leads to NO_3^- removal and adds ammonia, which has been measured in high abundance previously at CROMO (Crespo-Medina et al., 2014). All but one of the CROMO *Dethiobacter* bins have the complete pathway for this process, and two out of three *Serpentinomonas* bins and both *Truepera* bins also have genes for nitrate and nitrite reductases (Figure 4). Future studies should be focused on specifically evaluating the role of these nitrogen compounds as participants in bioenergetic reactions and as nutrient sources in serpentinizing systems.

4.4. Gas Exchange Within Terrestrial Serpentinizing Systems

CH_4 flux due to serpentinization at mid-ocean ridges was calculated to be 0.4 Megatons per kilometer of ridge axis (Cannat et al., 2013). The Chimaera gas seep in Turkey releases greater than 50 tons per year of a gas mixture, half of which is abiotic CH_4 influenced by low-temperature serpentinization (Hosgormez et al., 2008; Neubeck et al., 2017). However, microbial consumption of CH_4 can aid in regulating the quantity released to the atmosphere (Reeburgh, 2007). Earlier work at CROMO and other serpentinization-influenced sites has provided ambiguous interpretations of the origins of CH_4 due to overlapping abiotic, thermogenic, and microbial sources and sinks (Proskurowski et al., 2008; Wang et al., 2015), and inconsistent evidence of known methane cycling organisms. At the Cedars, the origin of methane remains unclear as isotopic data points at least partially to an abiotic source (Morrill et al., 2013) yet experimental evidence suggests the possibility of a microbial source (Kohl et al., 2016). In the Samail ophiolite, Oman, methane in fluids is isotopically heavy, and may have formed due to abiotic reduction of dissolved CO_2 or biotic pathways (Miller et al., 2016). Methanogens and methanotrophs have both been identified in the Oman wells, which may also contribute to the isotopic signatures detected there (Fones et al., 2019; Miller et al., 2016).

At CROMO, H_2 CO, and CH_4 generated by serpentinization processes have higher concentrations in the subsurface, and CO and H_2 are depleted prior to reaching the top of the CSW1.1 water column. CO can be used by *Serpentinomonas* (aerobic) and *Dethiobacter* (anaerobic), ultimately suppressing the quantities of measurable CO in the fluids. CH_4 may be used by putative methanotrophs present at low relative abundance in the 16S rRNA amplicon data, but more work would need to confirm the activity and impact of these populations on bulk biogeochemistry. The ~200 μM CH_4 measured at the top of the water column indicates CH_4 could potentially be released to the atmosphere (relative to the ~100 μM CH_4 in the air), and its concentration suggests that the gas is not fully scrubbed by resident microorganisms. While gas flux out of CSW1.1 was not explicitly quantified in this study, diffuse methane fluxes have been measured at other serpentinizing terranes (e.g., Etiope, Tsikouras, et al., 2013). Furthermore, the undersaturation of groundwater with respect to CO_2 and O_2 is likely to drive diffusion of these compounds into the aqueous phase. When comparing current atmospheric O_2 levels (20.95% of atmospheric gases; ~300 μM O_2) to measured values just below the top of the water column (300 μM at 100% O_2; ~150 μM at 50% O_2), O_2 at the air-water interface would dissolve into the water. Atmospheric CO_2 could also infiltrate into the groundwater and

contribute to higher DIC levels in the upper portions of the well. At pH 12, almost all DIC is present as CO_3^{2-} (or a complexed form), meaning any CO_2 that dissolves into the water is rapidly converted to CO_3^{2-}.

Work by Kelemen and Matter (2008) showed that atmospheric CO_2 could be captured and stored in the subsurface through the carbonation of peridotite. In Oman, for example, adding 1 wt% CO_2 to the area consisting of mantle peridotite could trap 25% of global atmospheric CO_2. Work at the Tablelands ophiolite in Newfoundland, Canada examined the impact of a serpentinizing system on both CO_2 sequestration and also CH_4 emissions (Morrissey & Morrill, 2017). They found that CO_2 flux was equal to 4.6×10^{-7} mol/(m^2·min) and CH_4 flux was 1.9×10^{-5} mol/(m^2·min), respectively. After accounting for the powerful greenhouse gas effect of CH_4 to that of CO_2, they identified that their ultrabasic pools were sequestering more CO_2 than CH_4 emission, which over a 100-year time span had a net cooling effect on the atmosphere (Morrissey & Morrill, 2017). In future work, accurately measuring net gas fluxes and fully unraveling the physical, chemical, and biological factors influencing them at CROMO and other serpentinizing terranes will be important for elucidating their impact on atmospheric concentrations of greenhouse gases.

5. Conclusions

This novel profile study of a monitoring well sampling an ultrabasic aquifer revealed how the products of serpentinization can be used by resident microbial communities to shape the biogeochemical gradients measured. While CH_4 coupled to O_2 provided the most energy per liter of fluid, the relevant genes for performing this reaction were not detected. Rather, genes in metabolic pathways related to the transformation of NO_3^-, NO_2^-, H_2, and CO were abundant despite low concentrations, indicating that microbial communities play a role in the chemical gradients measured, and the most abundant chemistries are not necessarily what is used for microbial metabolism. The three dominant organisms in CSW1.1, *Serpentinomonas*, *Truepera*, and *Dethiobacter* play a key role in cycling these lower abundance compounds and products of serpentinization, and influence the gradients observed with depth. Combined, this work lends new insight into the relationship between geochemical gradients, energy, and microbial communities in this extreme environment. Ultimately, this work reveals how these intricate biogeochemical relationships have the potential to impact the net exchange of CH_4, O_2 and CO_2 gases between the atmosphere and subsurface, which has important implications for Earth's carbon cycle and potentially climate. As each serpentinizing system is unique, it will be important to quantify the flux of these gases to gain a better perspective of their global impact and long-term controls on their emission.

Conflict of Interest

The authors declare no conflicts of interest relevant to this study.

Data Availability Statement

Table 1 data is publicly available in the PANGAEA repository: https://doi.org/10.1594/PANGAEA.931692. The 16S rRNA gene sequence data from the CROMO CSW1.1 depth profile are publicly available in the NCBI Sequence Read Archive (SRA) under project number PRJNA672823 and specific accession numbers SRX9385042 - SRX9385044, SRX9385047 - SRX9385048, and SRX9385050 - SRX9385053. *R* scripts used identify potential contaminant OTUs (doi.org/10.6084/m9.figshare.14036021) and to calculate downstream diversity metrics (doi.org/10.6084/m9.figshare.14036033) are available on Figshare. Excel files containing raw count data (doi.org/10.6084/m9.figshare.14524065), raw taxonomy data (doi.org/10.6084/m9.figshare.14524098), raw fasta sequences (doi.org/10.6084/m9.figshare.14524119), and meta data used for contaminant removal in *R* (doi.org/10.6084/m9.figshare.14524110) are also available on Figshare.

CROMO CSW1.1 depth profile metagenome sequences are publicly available in the SRA database under the the BioProject accession PRJNA672823 (SRX9385611 - SRX9385617), https://www.ncbi.nlm.nih.gov/bioproject/?term=PRJNA672823. Metagenome assembled genome (MAG) bin information was submitted to GenBank and is publicly available under the same project number above (PRJNA672823; accession numbers JAGXQU000000000 - JAGXTN000000000). MAG data for *Serpentinomonas*, *Truepera,* and select *Dethiobacter* bins are included in Seyler et al. (2020) and its supporting information files.

All other information related to the results are included in this manuscript as supporting tables and data sheets, and are also uploaded to Figshare for accessibility at the following DOIs: Data Set S1: doi.org/10.6084/m9.figshare.14035952; Data Set S2: doi.org/10.6084/m9.figshare.14035961; Data Set S3: doi.org/10.6084/m9.figshare.14035970; Data Set S4: doi.org/10.6084/m9.figshare.14035976; Data Set S5: doi.org/10.6084/m9.figshare.14035979; Data Set S6: doi.org/10.6084/m9.figshare.14035982; Data Set S7: doi.org/10.6084/m9.figshare.14489190; Table S1: doi.org/10.6084/m9.figshare.14035991; Table S2: doi.org/10.6084/m9.figshare.14035994; Table 2: doi.org/10.6084/m9.figshare.14035988.

Acknowledgments
The authors would like to thank Cathy Koehler and Paul Aigner, Directors of the University of California-Davis McLaughlin Natural Reserve for their support and guidance during field sampling. We are grateful to Tom McCollom for Gibbs energy calculation guidance and extremely helpful feedback on this manuscript. Thanks to Abdulmehdi Ali at the University of New Mexico for ICP-OES analyses, and the Zarnetske Lab at Michigan State University for performing IC analyses. Thanks to Christopher Thornton for the construction of metagenome libraries. Thanks to the entire May 2016 CROMO field team for extra assistance with this profiling work. This project was additionally supported by a NASA Astrobiology Institute 2016 Early Career Collaboration Award to M.C.S.

References

Albuquerque, L., Simoes, C., Nobre, M. F., Pino, N. M., Battista, J. R., Silva, M. T., et al. (2005). *Truepera radiovictrix* gen. nov., sp. nov., a new radiation resistant species and the proposal of Trueperaceae fam. nov. *FEMS Microbiology Letters*, *247*, 161–169. https://doi.org/10.1016/j.femsle.2005.05.002

Aloupi, M., Koutrotsios, G., Koulousaris, M., & Kalogeropoulos, N. (2012). Trace metal contents in wild edible mushrooms growing on serpentine and volcanic soils on the island of Lesvos, Greece. *Ecotoxicology and Environmental Safety*, *78*, 184–194. https://doi.org/10.1016/j.ecoenv.2011.11.018

Amend, J. P., & Shock, E. L. (2001). Energetics of overall metabolic reactions of thermophilic and hyperthermophilic Archaea and bacteria. *FEMS Microbiology Reviews*, *25*(2), 175–243. https://doi.org/10.1111/j.1574-6976.2001.tb00576.x

Arkin, A. P., Cottingham, R. W., Henry, C. S., Harris, N. L., Stevens, R. L., Maslov, S., et al. (2018). KBase: The United States department of energy systems biology knowledgebase. *Nature Biotechnology*, *36*(7), 566–569. https://doi.org/10.1038/nbt.4163

Baes, C. F., III, & McLaughlin, S. B. (1987). Trace metal uptake and accumulation in trees as affected by environmental pollution (Vol. G16). NATO ASI Series.

Beal, E. J., House, C. H., & Orphan, V. J. (2009). Manganese- and iron- dependent marine methane oxidation. *Science*, *325*, 184–187. https://doi.org/10.1126/science.1169984

Bell, E., Lamminmäki, T., Alneberg, J., Andersson, A. F., Qian, C., Xiong, W., et al. (2018). Biogeochemical cycling by a low-diversity microbial community in deep groundwater. *Frontiers in Microbiology*, *9*, 1–17. https://doi.org/10.3389/fmicb.2018.02129

Boisvert, S., Raymond, F., Godzaridis, E., Laviolette, F., & Corbeil, J. (2012). Ray Meta: Scalable de novo metagenome assembly and profiling. *Genome Biology*, *13*(12), R122. https://doi.org/10.1186/gb-2012-13-12-r122

Bowers, R. M., Kyrpides, N. C., Stepanauskas, R., Harmon-Smith, M., Doud, D., Reddy, T. B. K., et al. (2017). Minimum information about a single amplified genome (MISAG) and a metagenome-assembled genome (MIMAG) of bacteria and archaea. *Nature Biotechnology*, *35*(8), 725–731. https://doi.org/10.1038/nbt.3893

Bowman, J. P., Sly, L. T., Nichols, P. D., & Hayward, A. C. (1993). Revised taxonomy of the methanotrophs: Description of *Methylobacter* gen. nov., emendation of *Methylococcus*, validation of *Methylosinus* and *Methylocystis* species, and a proposal that the family Methylococcaceae includes only the group I Methanogens. *International Journal of Systematic Bacteriology*, *44*(2). https://doi.org/10.1099/00207713-44-2-375

Brazelton, W. J., Morrill, P. L., Szponar, N., & Schrenk, M. O. (2013). Bacterial communities associated with subsurface geochemical processes in continental serpentinite springs. *Applied and Environmental Microbiology*, *79*(13), 3906–3916. https://doi.org/10.1128/AEM.00330-13

Brazelton, W. J., Nelson, B., & Schrenk, M. O. (2012). Metagenomic evidence for H_2 oxidation and H_2 production by serpentinite-hosted subsurface microbial communities. *Frontiers in Microbiology*, *2*, 1–16. https://doi.org/10.3389/fmicb.2011.00268

Brazelton, W. J., Schrenk, M. O., Kelley, D. S., & Baross, J. A. (2006). Methane- and sulfur-metabolizing microbial communities dominate the Lost City Hydrothermal Field ecosystem. *Applied and Environmental Microbiology*, *72*(9), 6257–6270. https://doi.org/10.1128/AEM.00574-06

Brazelton, W. J., Thornton, C. N., Hyer, A., Twing, K. I., Longino, A. A., Lang, S. Q., et al. (2017). Metagenomic identification of active methanogens and methanotrophs in serpentinite springs of the Voltri Massif, Italy. *PeerJ*, *5*, e2945. https://doi.org/10.7717/peerj.2945

Buchfink, B., Xie, C., & Huson, D. H. (2014). Fast and sensitive protein alignment using DIAMOND. *Nature Methods*, *12*(1), 59–60. https://doi.org/10.1038/nmeth.3176

Cannat, M., Fontaine, F., & Escartin, J. (2013). Serpentinization and associated hydrogen and methane fluxes at slow spreading ridges. In *Diversity of hydrothermal systems on slow spreading ocean ridges*. https://doi.org/10.1029/2008GM000760

Canovas, P. A., Hoehler, T., & Shock, E. L. (2017). Geochemical bioenergetics during low-temperature serpentinization: An example from the Samail ophiolite, Sultanate of Oman. *Journal of Geophysical Research: Biogeosciences*, *122*(7), 1821–1847. https://doi.org/10.1002/2017JG003825

Cardace, D., Meyer-Dombard, D. R., Woycheese, K. M., & Arcilla, C. A. (2015). Feasible metabolisms in high pH springs of the Philippines. *Frontiers in Microbiology*, *6*, 1–10. https://doi.org/10.3389/fmicb.2015.00010

Chaumeil, P.-A., Mussig, A. J., Hugenholtz, P., & Parks, D. H. (2019). GTDB-Tk: A toolkit to classify genomes with the Genome Taxonomy Database. *Bioinformatics*, *36*, 1925–1927. https://doi.org/10.1093/bioinformatics/btz848

Chavagnac, V., Ceuleneer, G., Monnin, C., Lansac, B., Hoareau, G., & Boulart, C. (2013). Mineralogical assemblages forming at hyperalkaline warm springs hosted on ultramafic rocks: A case study of Oman and Ligurian ophiolites. *Geochemistry, Geophysics, Geosystems*, *14*(7), 2474–2495. https://doi.org/10.1002/ggge.20146

Cline, J. D. (1969). Spectrophotometric determination of hydrogen sulfide in natural waters. *Limnology and Oceanography*, *14*, 454–458. https://doi.org/10.4319/lo.1969.14.3.0454

Crespo-Medina, M., Twing, K. I., Kubo, M. D. Y., Hoehler, T. M., Cardace, D., McCollom, T., & Schrenk, M. O. (2014). Insights into environmental controls on microbial communities in a continental serpentinite aquifer using a microcosm-based approach. *Frontiers in Microbiology*, *5*, 604. https://doi.org/10.3389/fmicb.2014.00604

Crespo-Medina, M., Twing, K. I., Sánchez-Murillo, R., Brazelton, W. J., McCollom, T. M., & Schrenk, M. O. (2017). Methane dynamics in a tropical serpentinizing environment: The Santa Elena Ophiolite, Costa Rica. *Frontiers in Microbiology*, *8*, 1–14. https://doi.org/10.3389/fmicb.2017.00916

Edgar, R. C. (2010). Search and clustering orders of magnitude faster than BLAST. *Bioinformatics*, *26*(19), 2460–2461. https://doi.org/10.1093/bioinformatics/btq461

Edgar, R. C., Haas, B. J., Clemente, J. C., Quince, C., & Knight, R. (2011). UCHIME improves sensitivity and speed of chimera detection. *Bioinformatics*, *27*(16), 2194–2200. https://doi.org/10.1093/bioinformatics/btr381

Eren, A. M., Esen, O. C., Quince, C., Vineis, J. H., Morrison, H. G., Sogin, M. L., & Delmont, T. O. (2015). Anvi'o: An advanced analysis and visualization platform for 'omics data. *PeerJ*, *3*(10), 1–29. https://doi.org/10.7717/peerj.1319

Etiope, G., Ehlmann, B. L., & Schoell, M. (2013). Low temperature production and exhalation of methane from serpentinized rocks on Earth: A potential analog for methane production on Mars. *Icarus*, *224*(2), 276–285. https://doi.org/10.1016/j.icarus.2012.05.009

Etiope, G., Tsikouras, B., Kordella, S., Ifandi, E., Christodoulou, D., & Papatheodorou, G. (2013). Methane flux and origin in the Othrys ophiolite hyperalkaline springs, Greece. *Chemical Geology*, *347*, 161–174. https://doi.org/10.1016/j.chemgeo.2013.04.003

Fones, E. M., Colman, D. R., Kraus, E. A., Nothaft, D. B., Poudel, S., Rempfert, K. R., et al. (2019). Physiological adaptations to serpentinization in the Samail Ophiolite, Oman. *ISME Journal*, *13*, 1750–1762. https://doi.org/10.1038/s41396-019-0391-2

Fones, E. M., Colman, D. R., Kraus, E. A., Stepanauskas, R., Templeton, A. S., Spear, J. R., & Boyd, E. S. (2020). Diversification of methanogens into hyperalkaline serpentinizing environments through adaptations to minimize oxidant limitation. *ISME Journal*, *15*, 22–1135. https://doi.org/10.1038/s41396-020-00838-1

Fullerton, K. M., Schrenk, M. O., Yücel, M., Manini, E., Basili, M., Rogers, T. J., et al. (2021). Effect of tectonic processes on biosphere-geosphere feedbacks across a convergent margin. *Nature Geoscience*, *14*, 301–306. https://doi.org/10.1038/s41561-021-00725-0

Graham, E. D., Heidelberg, J. F., & Tully, B. J. (2017). Binsanity: Unsupervised clustering of environmental microbial assemblies using coverage and affinity propagation. *PeerJ*, *5*(3), 1–19. https://doi.org/10.7717/peerj.3035

Greening, C., Biswas, A., Carere, C. R., Jackson, C. J., Taylor, M. C., Stott, M. B., et al. (2016). Genomic and metagenomic surveys of hydrogenase distribution indicate H_2 is a widely utilised energy source for microbial growth and survival. *ISME Journal*, *10*(3), 761–777. https://doi.org/10.1038/ismej.2015.153

Hoehler, T. M., Alperin, M. J., Albert, D. B., & Martens, C. S. (2001). Apparent minimum free energy requirements for methanogenic Archaea and sulfate-reducing bacteria in an anoxic marine sediment. *FEMS Microbiology Ecology*, *38*(1), 33–41. https://doi.org/10.1016/S0168-6496(01)00175-1

Holloway, J. M., Goldhaber, M. B., Scow, K. M., & Drenovsky, R. E. (2009). Spatial and seasonal variations in mercury methylation and microbial community structure in a historic mercury mining area, Yolo County, California. *Chemical Geology*, *267*(1–2), 85–95. https://doi.org/10.1016/j.chemgeo.2009.03.031

Hoppe, T., Peters, K., & Schmidt, F. (2011). *Methylobacterium bullatum* sp. nov., a methylotrophic bacterium isolated from *Funaria hygrometrica*. *Systematic and Applied Microbiology*, *34*(7), 482–486. https://doi.org/10.1016/j.syapm.2010.12.005

Hosgormez, H., Etiope, G., & Yalçin, M. N. (2008). New evidence for a mixed inorganic and organic origin of the Olympic Chimaera fire (Turkey): A large onshore seepage of abiogenic gas. *Geofluids*, *8*(4), 263–273. https://doi.org/10.1111/j.1468-8123.2008.00226.x

Hyatt, D., Chen, G.-L., Locascio, P. F., Land, M. L., Larimer, F. W., & Hauser, L. J. (2010). Prodigal: Prokaryotic gene recognition and translation initiation site identification. *BMC Bioinformatics*, *11*, 119. https://doi.org/10.1186/1471-2105-11-119

Jones, I., & Lerner, D. N. (1995). Level-determined sampling in an uncased borehole. *Journal of Hydrology*, *171*(3–4), 291–317. https://doi.org/10.1016/0022-1694(95)06015-B

Joye, S. B., Connell, T. L., Miller, L. G., Oremland, R., & Jellison, R. S. (1999). Oxidation of ammonia and methane in an alkaline, saline lake. *Limnology and Oceanography*, *44*(1), 178–188. https://doi.org/10.4319/lo.1999.44.1.0178

Kanehisa, M., Sato, Y., & Morishima, K. (2016). BlastKOALA and GhostKOALA: KEGG tools for functional characterization of genome and metagenome sequences. *Journal of Molecular Biology*, *428*(4), 726–731. https://doi.org/10.1016/j.jmb.2015.11.006

Kappler, A., & Bryce, C. (2017). Cryptic biogeochemical cycles: Unravelling hidden redox reactions. *Environmental Microbiology*, *19*(3), 842–846. https://doi.org/10.1111/1462-2920.13687

Kelemen, P. B., & Matter, J. (2008). In situ carbonation of peridotite for CO_2 storage. *Proceedings of the National Academy of Sciences of the United States of America*, *105*(45), 17295–17300. https://doi.org/10.1073/pnas.0805794105

Kohl, L., Cumming, E., Cox, A., Rietze, A., Morrissey, L., Lang, S. Q., et al. (2016). Exploring the metabolic potential of microbial communities in ultra-basic, reducing springs at The Cedars, CA, USA. *Journal of Geophysical Research: Biogeosciences*, *121*, 1203–1220. https://doi.org/10.1002/2015JG003233

Kozich, J. J., Westcott, S. L., Baxter, N. T., Highlander, S. K., & Schloss, P. D. (2013). Development of a dual-index sequencing strategy and curation pipeline for analyzing amplicon sequence data on the MiSeq Illumina sequencing platform. *Applied and Environmental Microbiology*, *79*(17), 5112–5120. https://doi.org/10.1128/AEM.01043-13

Kraus, E. A., Nothaft, D., Stamps, B. W., Rempfert, K. R., Ellison, E. T., Matter, J. M., et al. (2021). Molecular evidence for an active microbial methane cycle in subsurface serpentinite-hosted groundwaters in the Samail Ophiolite, Oman. *Applied and Environmental Microbiology*, *87*(2). https://doi.org/10.1128/aem.02068-20

Langmead, B., & Salzberg, S. L. (2012). Fast gapped-read alignment with Bowtie 2. *Nature Methods*, *9*(4), 357–359. https://doi.org/10.1038/nmeth.1923.Fast

Li, D., Luo, R., Liu, C. M., Leung, C. M., Ting, H. F., Sadakane, K., et al. (2016). MEGAHIT v1.0: A fast and scalable metagenome assembler driven by advanced methodologies and community practices. *Methods*, *102*, 3–11. https://doi.org/10.1016/j.ymeth.2016.02.020

Li, H., Handsaker, B., Wysoker, A., Fennell, T., Ruan, J., Homer, N., et al. (2009). The sequence alignment/map format and SAMtools. *Bioinformatics*, *25*(16), 2078–2079. https://doi.org/10.1093/bioinformatics/btp352

Liedert, C., Peltola, M., Bernhardt, J., Neubauer, P., & Salkinoja-Salonen, M. (2012). Physiology of resistant *Deinococcus geothermalis* bacterium aerobically cultivated in low-manganese medium. *Journal of Bacteriology*, *194*(6), 1552–1561. https://doi.org/10.1128/JB.06429-11

Ludwig, W., Strunk, O., Westram, R., Richter, L., Meier, H., Yadhukumar, A., et al. (2004). ARB: A software environment for sequence data. *Nucleic Acids Research*, *32*(4), 1363–1371. https://doi.org/10.1093/nar/gkh293

Mayhew, L. E., Ellison, E. T., McCollom, T. M., Trainor, T. P., & Templeton, A. (2013). Hydrogen generation from low-temperature water-rock reactions. *Nature Geoscience*, *6*(6), 478–484. https://doi.org/10.1038/NGEO1825

McCollom, T. M., & Seewald, J. S. (2013). Serpentinites, hydrogen, and life. *Elements*, *9*(2), 129–134. https://doi.org/10.2113/gselements.9.2.129

McCollom, T. M., & Shock, E. L. (1997). Geochemical constraints on chemolithoautotrophic metabolism by microorganisms in seafloor hydrothermal systems. *Geochimica et Cosmochimica Acta*, *61*(20), 4375–4391. https://doi.org/10.1016/S0016-7037(97)00241-X

McGonigle, J. M., Lang, S. Q., & Brazelton, W. J. (2020). Genomic evidence for formate metabolism by *Chloroflexi* as the key to unlocking deep carbon in Lost City microbial ecosystems. *Applied and Environmental Microbiology*, *86*, 1–12. https://doi.org/10.1128/aem.02583-19

McKay, C. P., Anbar, A. D., Porco, C., & Tsou, P. (2014). Follow the plume: The habitability of Enceladus. *Astrobiology*, *14*(4), 352–355. https://doi.org/10.1089/ast.2014.1158

Merino, N., Kawai, M., Boyd, E. S., Colman, D. R., McGlynn, S. E., Nealson, K. H., et al. (2020). Single-cell genomics of novel actinobacteria with the wood–Ljungdahl Pathway Discovered in a Serpentinizing System. *Frontiers in Microbiology*, *11*, 1–21. https://doi.org/10.3389/fmicb.2020.01031

Meyer-Dombard, D. R., Woycheese, K. M., Yargicoglu, E. N., Cardace, D., Shock, E. L., Gulecal-Pektas, Y., & Temel, M. (2015). High pH microbial ecosystems in a newly discovered, ephemeral, serpentinizing fluid seep at Yanartas (Chimera), Turkey. *Frontiers in Microbiology*, *6*, 1–13. https://doi.org/10.3389/fmicb.2014.00723

Miller, H. M., Matter, J. M., Kelemen, P., Ellison, E. T., Conrad, M. E., Fierer, N., et al. (2016). Modern water/rock reactions in Oman hyperalkaline peridotite aquifers and implications for microbial habitability. *Geochimica et Cosmochimica Acta*, *179*, 217–241. https://doi.org/10.1016/j.gca.2016.01.033

Monnin, C., Chavagnac, V., Boulart, C., Ménez, B., Gérard, M., Gérard, E., et al. (2014). Fluid chemistry of the low temperature hyperalkaline hydrothermal system of Prony bay (New Caledonia). *Biogeosciences*, *11*(20), 5687–5706. https://doi.org/10.5194/bg-11-5687-2014

Morrill, P. L., Brazelton, W. J., Kohl, L., Rietze, A., Miles, S. M., Kavanagh, H., et al. (2014). Investigations of potential microbial methanogenic and carbon monoxide utilization pathways in ultra-basic reducing springs associated with present-day continental serpentinization : The Tablelands, NL, CAN. *Frontiers in Microbiology*, *5*, 1–13. https://doi.org/10.3389/fmicb.2014.00613

Morrill, P. L., Kuenen, J. G., Johnson, O. J., Suzuki, S., Rietze, A., Sessions, A. L., et al. (2013). Geochemistry and geobiology of a present-day serpentinization site in California: The Cedars. *Geochimica et Cosmochimica Acta*, *109*, 222–240. https://doi.org/10.1016/j.gca.2013.01.043

Morrissey, L. S., & Morrill, P. L. (2017). Flux of methane release and carbon dioxide sequestration at Winterhouse Canyon, Gros Morne, Newfoundland, Canada: A site of continental serpentinization. *Canadian Journal of Earth Sciences*, *54*(3), 257–262. https://doi.org/10.1139/cjes-2016-0123

Motamedi, S., Orcutt, B. N., Früh-Green, G. L., Twing, K. I., Pendleton, H. L., & Brazelton, W. J. (2020). Microbial residents of the Atlantis Massif's shallow serpentinite subsurface. *Applied and Environmental Microbiology*, *86*. https://doi.org/10.1128/AEM.00356-20

Neubeck, A., Sun, L., Müller, B., Ivarsson, M., Hosgörmez, H., Özcan, D., et al. (2017). Microbial community structure in a serpentine-hosted abiotic gas seepage at the Chimaera Ophiolite, Turkey. *Applied and Environmental Microbiology*, *83*, 1–17. https://doi.org/10.1128/aem.03430-16

Ogata, H., Goto, S., Sato, K., Fujibuchi, W., Bono, H., & Kanehisa, M. (1999). KEGG: Kyoto encyclopedia of genes and genomes. *Nucleic Acids Research*, *27*(1), 29–34. Retrieved from http://www.kegg.jp/

Oksanen, J., Blanchet, F. G., Friendly, M., Kindt, R., Legendre, P., McGlinn, D., et al. (2019). vegan: Community Ecology Package 2.5-6.

Orphan, V. J., House, C. H., Hinrichs, K.-U., McKeegan, K. D., & DeLong, E. F. (2002). Multiple archeal groups mediate methane oxidation in anoxic cold seep sediments. *Proceedings of the National Academy of Sciences of the United States of America*, *99*(11), 7663–7668. https://doi.org/10.1073/pnas.072210299

Ortiz, E., Tominaga, M., Cardace, D., Schrenk, M. O., Hoehler, T. M., Kubo, M. D., & Rucker, D. F. (2018). Geophysical characterization of serpentinite hosted hydrogeology at the McLaughlin Natural Reserve, Coast Range Ophiolite. *Geochemistry, Geophysics, Geosystems*, *19*(1), 114–131. https://doi.org/10.1002/2017GC007001

Parks, D. H., Imelfort, M., Skennerton, C. T., Hugenholtz, P., & Tyson, G. W. (2015). CheckM: Assessing the quality of microbial genomes recovered from isolates, single cells, and metagenomes. *Genome Research*, *25*(7), 1043–1055. https://doi.org/10.1101/gr.186072.114

Peters, J. W., Schut, G. J., Boyd, E. S., Mulder, D. W., Shepard, E. M., Broderick, J. B., et al. (2015). [FeFe]- and [NiFe]-hydrogenase diversity, mechanism, and maturation. *Biochimica et Biophysica Acta (BBA) - Molecular Cell Research*, *1853*(6), 1350–1369. https://doi.org/10.1016/j.bbamcr.2014.11.021

Proskurowski, G., Lilley, M. D., Seewald, J. S., Früh-Green, G. L., Olson, E. J., Lupton, J. E., et al. (2008). Abiogenic hydrocarbon production at Lost City Hydrothermal Field. *Science (New York, N.Y.)*, *319*(5863), 604–607. https://doi.org/10.1126/science.1151194

Pruesse, E., Quast, C., Knittel, K., Fuchs, B. M., Ludwig, W., Peplies, J., & Glöckner, F. O. (2007). SILVA: A comprehensive online resource for quality checked and aligned ribosomal RNA sequence data compatible with ARB. *Nucleic Acids Research*, *35*(21), 7188–7196. https://doi.org/10.1093/nar/gkm864

Quéméneur, M., Bes, M., Postec, A., Mei, N., Hamelin, J., Monnin, C., et al. (2014). Spatial distribution of microbial communities in the shallow submarine alkaline hydrothermal field of the Prony Bay, New Caledonia. *Environmental Microbiology Reports*, *6*(6), 665–674. https://doi.org/10.1111/1758-2229.12184

R Core Team (2019). *R: A language and environment for statistical computing*. Vienna, Austria. R Foundation for Statistical Computing. Retrieved from https://www.R-project.org/

Reeburgh, W. (2007). Oceanic methane biogeochemistry. *American Chemical Society*, *107*(2), 486–513. https://doi.org/10.1021/cr050362v

Rempfert, K. R., Miller, H. M., Bompard, N., Nothaft, D., Matte, J. M., Kelemen, P., et al. (2017). Geological and geochemical controls on subsurface microbial life in the Samail Ophiolite, Oman. *Frontiers in Microbiology*, *8*(56), 1–21. https://doi.org/10.3389/fmicb.2017.00056

Rohland, N., & Reich, D. (2012). Cost-effective, high-throughput DNA sequencing libraries for multiplexed target capture. *Genome Research*, *22*(5), 939–946. https://doi.org/10.1101/gr.128124.111

Sabuda, M. C., Brazelton, W. J., Putman, L. I., McCollom, T. M., Hoehler, T. M., Kubo, M. D. Y., et al. (2020). A dynamic microbial sulfur cycle in a serpentinizing continental ophiolite. *Environmental Microbiology*, *22*, 2329–2345. https://doi.org/10.1111/1462-2920.15006

Sanchez-Murillo, R., Gazel, E., Schwarzenbach, E. M., Crespo-Medina, M., Schrenk, M. O., Boll, J., & Gill, B. C. (2014). Geochemical evidence for active tropical serpentinization in the Santa Elena Ophiolite, Costa Rica: An analog of a humid early Earth? *Geochemistry, Geophysics, Geosystems*, *18*, 1–16. https://doi.org/10.1002/2014GC005356

Schink, B. (1997). Energetics of syntrophic cooperation in methanogenic degradation. *Microbiology and Molecular Biology Reviews*, *61*(2), 262–280. https://doi.org/10.1128/.61.2.262-280.1997

Schloss, P. D., & Westcott, S. L. (2011). Assessing and improving methods used in operational taxonomic unit-based approaches for 16S rRNA gene sequence analysis. *Applied and Environmental Microbiology*, *77*(10), 3219–3226. https://doi.org/10.1128/AEM.02810-10

Schloss, P. D., Westcott, S. L., Ryabin, T., Hall, J. R., Hartmann, M., Hollister, E. B., et al. (2009). Introducing mothur: Open-source, platform-independent, community-supported software for describing and comparing microbial communities. *Applied and Environmental Microbiology*, *75*(23), 7537–7541. https://doi.org/10.1128/AEM.01541-09

Schrenk, M. O., Brazelton, W. J., & Lang, S. Q. (2013). Serpentinization, carbon, and deep life. *Reviews in Mineralogy*, *75*, 575–606. https://doi.org/10.2138/rmg.2013.75.18

Schrenk, M. O., Kelley, D. S., Delaney, J. R., & Baross, J. A. (2003). Incidence and diversity of microorganisms within the walls of an active deep-sea sulfide chimney. *Applied and Environmental Microbiology*, *69*(6), 3580–3592. https://doi.org/10.1128/AEM.69.6.3580-3592.2003

Schwarzenbach, E. M., Früh-Green, G. L., Bernasconi, S. M., Alt, J. C., Shanks, W. C., Gaggero, L., & Crispini, L. (2012). Sulfur geochemistry of peridotite-hosted hydrothermal systems: Comparing the Ligurian ophiolites with oceanic serpentinites. *Geochimica et Cosmochimica Acta*, *91*, 283–305. https://doi.org/10.1016/j.gca.2012.05.021

Schwarzenbach, E. M., Gill, B. C., Gazel, E., & Madrigal, P. (2016). Sulfur and carbon geochemistry of the Santa Elena peridotites: Comparing oceanic and continental processes during peridotite alteration. *Lithos*, *252–253*, 92–108. https://doi.org/10.1016/j.lithos.2016.02.017

Seyler, L. M., Brazelton, W. J., McLean, C., Putman, L. I., Hyer, A., Kubo, M. D. Y., et al. (2020). Carbon assimilation strategies in ultrabasic groundwater: clues from the integrated study of a serpentinization-influenced aquifer. *MSystems*, *5*(2), 1–17. https://doi.org/10.1128/mSystems.00607-19

Sheik, C. S., Reese, B. K., Twing, K. I., Sylvan, J. B., Grim, S. L., Schrenk, M. O., et al. (2018). Identification and removal of contaminant sequences from ribosomal gene databases: Lessons from the Census of Deep Life. *Frontiers in Microbiology*, *9*, 1–14. https://doi.org/10.3389/fmicb.2018.00840

Sivan, O., Adler, M., Pearson, A., Gelman, F., Bar-Or, I., John, S. G., & Eckert, W. (2011). Geochemical evidence for iron-mediated anaerobic oxidation of methane. *Limnology and Oceanography*, *56*(4), 1536–1544. https://doi.org/10.4319/lo.2011.56.4.1536

Søndergaard, D., Pedersen, C. N. S., & Greening, C. (2016). HydDB: A web tool for hydrogenase classification and analysis. *Scientific Reports*, *6*, 1–8. https://doi.org/10.1038/srep34212

Suda, K., Ueno, Y., Yoshizaki, M., Nakamura, H., Kurokawa, K., Nishiyama, E., et al. (2014). Origin of methane in serpentinite-hosted hydrothermal systems: The CH_4-H_2-H_2O hydrogen isotope systematics of the Hakuba Happo hot spring. *Earth and Planetary Science Letters*, *386*, 112–125. https://doi.org/10.1016/j.epsl.2013.11.001

Suzuki, S., Ishii, S., Wu, A., Cheung, A., Tenney, A., Wanger, G., et al. (2013). Microbial diversity in The Cedars, an ultrabasic, ultrareducing, and low salinity serpentinizing ecosystem. *Proceedings of the National Academy of Sciences of the United States of America*, *110*(38), 15336–15341. https://doi.org/10.1073/pnas.1302426110

Suzuki, S., Kuenen, J. G., Schipper, K., van der Velde, S., Ishii, S., Wu, A., et al. (2014). Physiological and genomic features of highly alkaliphilic hydrogen-utilizing Betaproteobacteria from a continental serpentinizing site. *Nature Communications*, *5*, 3900. https://doi.org/10.1038/ncomms4900

Szponar, N., Brazelton, W. J., Schrenk, M. O., Bower, D. M., Steele, A., & Morrill, P. L. (2013). Geochemistry of a continental site of serpentinization, the Tablelands Ophiolite, Gros Morne National Park: A Mars analogue. *Icarus*, *224*(2), 286–296. https://doi.org/10.1016/j.icarus.2012.07.004

Thornton, C. N., Tanner, W. D., VanDerslice, J. A., & Brazelton, W. J. (2020). Localized effect of treated wastewater effluent on the resistome of an urban watershed. *GigaScience*, *9*(11), 1–13. https://doi.org/10.1093/gigascience/giaa125

Twing, K. I., Brazelton, W. J., Kubo, M. D. Y., Hyer, A. J., Cardace, D., Hoehler, T., et al. (2017). Serpentinization-influenced groundwater harbors extremely low diversity microbial communities adapted to high pH. *Frontiers in Microbiology*, *8*, 308. https://doi.org/10.3389/FMICB.2017.00308

vanGrinsven, S., Sinninghe Damsté, J. S., Abdala Asbun, A., Engelmann, J. C., Harrison, J., & Villanueva, L. (2020). Methane oxidation in anoxic lake water stimulated by nitrate and sulfate addition. *Environmental Microbiology*, *22*(2), 766–782. https://doi.org/10.1111/1462-2920.14886

Wang, D. T., Gruen, D. S., Lollar, B. S., Hinrichs, K.-U., Stewart, L. C., Holden, J. F., et al. (2015). Methane cycling. Nonequilibrium clumped isotope signals in microbial methane. *Science (New York, N.Y.)*, *348*(6233), 428–431. https://doi.org/10.1126/science.aaa4326

Woycheese, K. M., Meyer-Dombard, D. R., Cardace, D., Argayosa, A. M., & Arcilla, C. A. (2015). Out of the dark: Transitional subsurface-to-surface microbial diversity in a terrestrial serpentinizing seep (Manleluag, Pangasinan, the Philippines). *Frontiers in Microbiology*, *6*, 1–12. https://doi.org/10.3389/fmicb.2015.00044